A Device for Debridement Using High Pressure Water Jets

by

Ashley Brown

Submitted to the Department of Mechanical Engineering
in partial fulfillment of the requirements for the degree of

Master of Science in Mechanical Engineering

at the

MASSACHUSETTS INSTITUTE OF TECHNOLOGY

June 2014

Signature redacted

Author .....
Department of Mechanical Engineering
May 27, 2014

Signature redacted

Certified by .....
Ian W. Hunter
Hatsopoulos Professor of Mechanical Engineering
Thesis Supervisor

Signature redacted

Accepted by .....
David E. Hardt
Chairman, Department Committee on Graduate Theses

A Device for Debridement Using High Pressure Water Jets

by

Ashley Brown

Submitted to the Department of Mechanical Engineering
on May 27, 2014, in partial fulfillment of the
requirements for the degree of
Master of Science in Mechanical Engineering

Abstract

Removing devitalized tissue from chronic wounds through debridement is critical to promote wound healing. In this thesis, technology using high-speed water jets is explored toward applications for debridement. After presenting possible techniques, the thesis expands on one promising method using two impinging cutting jets that is further developed and demonstrated on simulated necrotic tissue. Surgical blades are used to score the tissue in advance of the nozzles. Vacuum suction is applied to locally evacuate waste. At optimal parameters of 75 µm orifices spaced 2 mm apart at 110°, the device was able to excise soft necrotic tissue at 6 MPa. This configuration was able to make side-by-side excisions and caused no visible damage to the surrounding tissue. Furthermore, preliminary tests suggest that the device does not propagate bacteria into soft tissue. Suggestions for improvements to this technology are given, particularly with respect to accidental injection of water into cut tissue. The data suggests that the device shows promise as a debridement technique.

Thesis Supervisor: Ian W. Hunter
Title: Hatsopoulos Professor of Mechanical Engineering

Acknowledgments

First, I would like to thank my advisor Professor Ian Hunter for giving me to opportunity to work in his lab the past three years. I have learned a tremendous amount here and I am inspired on a daily basis.

I would also like to thank Dr. Cathy Hogan for her guidance and mentorship throughout this project. She continually pointed me towards key insights, guided me in the next step of experimentation, and trained me in the scientific process. My technical and investigative skills have substantially grown through her influence.

The members of the Bioinstrumentation lab, thank you both for your friendship and for sharing your considerable expertise. Thank you to Ashin Modak and John Liu for your efforts in editing this thesis, and to Brian Hemond and Mike Nawrot for your helpful insights. Kate, thank you for making the research a smooth and enjoyable process. Thank you Alison Cloutier for your friendship and encouragement.

This research was supported in part through the NSF Graduate Research Fellowship and 3M.

Thank you Marcel Thomas for motivating me to be a better engineer.

To my parents, I think you two are amazing and I am immensely grateful for all the support you have given me in every way. Thank you for introducing me to my God, who means everything to me.

Contents

Chapter 1

Introduction

The care of chronic wounds is a significant burden both on the healthcare system, costing $25 billion annually in the US [1], and on the patient, causing pain and limiting activity [2]. An estimated 3 to 6 million American are affected by chronic wounds, many of which are ulcers associated with restricted blood flow, diabetes mellitus, or pressure [3]. Treatment is frequently unsuccessful, with only an estimated 25 to 50% of venous and diabetic ulcers closing after twenty weeks of treatment [4].

Debridement, the removal of necrotic tissue and foreign materials from wounds, is a crucial component in chronic wound care [5]. While there exist many debridement techniques, the search for new and more effective methods is ongoing [6].

This thesis presents the development of a novel debridement device that uses two high speed jets to excise necrotic tissue. Chapter 2 gives background on wound care and the mechanics of cutting with jets. Chapter 3 describes the generation and testing of debridement concepts. Chapter 4 presents the design and performance of a two-nozzle device, and Chapter 5 details further tests with and improvements to this device. Finally, Chapter 6 discusses the device capabilities and future work.

Chapter 2

Background

2.1 Wound Healing Process

Human skin consists of two layers. The outer epidermis acts as a protective barrier, shielding the dermis beneath. In addition to nourishing the epidermis, the dermis provides a supporting structure through a collagen-rich extracellular matrix [7].

Acute wounds are breaches of the epidermis caused by trauma or surgery that heal in four overlapping stages [8][9]. After the initial tissue breach, the **coagulation** phase begins, during which a clot of platelets and cross-linked fibrin protein halt bleeding. In the **inflammation** phase, chemical signals attract inflammatory cells from the circulating blood. Neutrophils remove contaminating bacteria and macrophages clear the remains of damaged cells and matrix. **Cell proliferation** occurs when new capillaries penetrate the clot, allowing granulation tissue to form [7]. Fibroblasts fill the injury with a provisional wound matrix while epithelial cells multiply at the wound edge and migrate across the granulation tissue, forming a new epidermis [7]. Finally, **remodeling** continues for several weeks with synthesis of new extracellular matrix and apoptosis of unneeded cells. The wound healing process can take up to several months [8].

2.2 Chronic Wounds and Wound Bed Preparation

Chronic wounds fail to re-epithelialize and are locked in the inflammatory phase of wound healing [5][6]. In chronic wounds, devitalized tissue in the form of either a dry eschar or moist slough (Fig. 2-1) stimulates pro-inflammatory signals and blocks the migration of healthy cells into the wound bed [5]. This necrotic tissue provides a environment for bacterial proliferation, increasing the risk of infection [10].

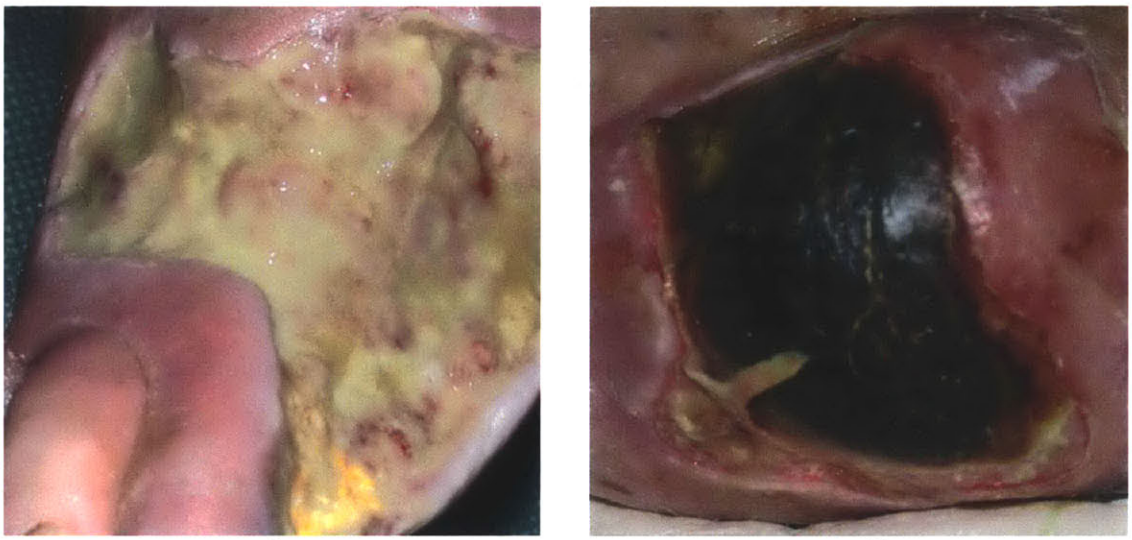

Figure 2-1: Two types of necrotic tissue. (A) is a wound with slough, a soft mass of devitalized tissue, frequently yellow in color. (B) shows a wound with dry and hard necrotic tissue, eschar. The redness surrounding this wound may indicate infection. Photos reproduced from [11].

An important concept in treating chronic wounds is wound bed preparation, the goal of which is to restore the environment of an acute wound by debridement, management of exudate, and regulation of the bacterial load [10]. The removal of devitalized tissue and foreign materials in conjunction with abundant lavage decreases the risk of infection [6].

2.2.1 Lavage

During lavage, a wound is irrigated with fluid in order to remove bacteria and particulates [5][12]. Lavage can be delivered at low pressures, generally defined as 9 to 100 kPa, or at high pressures between 240 and 480 kPa [12]. Although high pressure lavage can remove contaminants [13], the technique damages soft tissue [14]. Additionally, high pressure lavage drives bacteria to penetrate into soft tissue, leading many to recommend low pressure lavage as the preferred method for bacterial removal [12].

2.2.2 Debridement Techniques

Five well-established methods are used for debridement [6][5]:

Sharp Debridement is the excision of necrotic tissue with a scalpel or scissors [15]. Although considered the best technique for fast removal of large amounts of necrotic tissue, sharp debridement does not allow for selective removal of devitalized tissue [6]. Surgeons are taught to debride the wound until it bleeds [1], and blood loss is a problem in some patients [16]. Performing this technique requires training in surgical debridement [5] and is costly [17].

Mechanical Debridement involves placing wet-to-dry dressings on the wound. When the dry dressing is removed, so is the top layer of tissue. This method removes healthy as well as necrotic tissue and can be quite painful [18].

Autolytic Debridement uses the bodys own tissue-degrading enzymes to selectively break down necrotic tissue. Moist dressings are applied to wounds to stimulate production of these enzymes. This technique can be prohibitively slow [5].

Enzymatic Debridement is the introduction of enzymes such as collagenase to the wound bed in order to break down the damaged extracellular matrix [5].

Larval Therapy uses the sterile larvae of the green bottle fly to dissolve necrotic tissue using enzymes in their saliva. The maggots use the devitalized tissue as a food

source. Larval therapy is faster than autolytic debridement [19].

Each method has advantages and drawbacks which are summarized in Table 2.1. The most appropriate treatment depends on the patient, the wound, and the available resources [5].

Table 2.1: A comparison of common debridement techniques, where 1 is the most appropriate and 4 is the least appropriate. Adapted from [17].

	Autolytic	Surgical	Enzymatic	Mechanical
Speed	4	1	2	3
Tissue Selectivity	3	2	1	4
Painful Wound	1	4	2	3
Exudate	3	1	3	2
Infection	4	1	3	2
Cost	1	4	2	3

A relatively new debridement technique, **hydrosurgery**, uses a narrow saline jet to simultaneously lavage and debride soft tissue [20][21]. The Versajet^{TM} selectively removes necrotic tissue using a sterile saline jet directed parallel to the wound surface [21]. The high velocity stream causes a local decrease in pressure by the venturi effect, drawing the targeted tissue into the cutting path (Fig. 2-2). The device is lauded for its speed, ease of use, and ability to reduce bacterial load [22]. However, because the device relies on suction to deform tissue into the cutting path, it is unable to debride hard eschar. Furthermore, the technique's slow material removal rate makes it a poor choice for debriding deep burn wounds or other wounds with a large volume of necrotic tissue [20].

2.3 Cutting Mechanics and Fluid Jets

Shergold et al. showed that when a liquid jet breaches a soft material, it opens a planar crack, comparable to the behavior observed using sharp-tipped punches [25]. As illustrated in Fig. 2-3, the crack closes after the punch is removed. A review

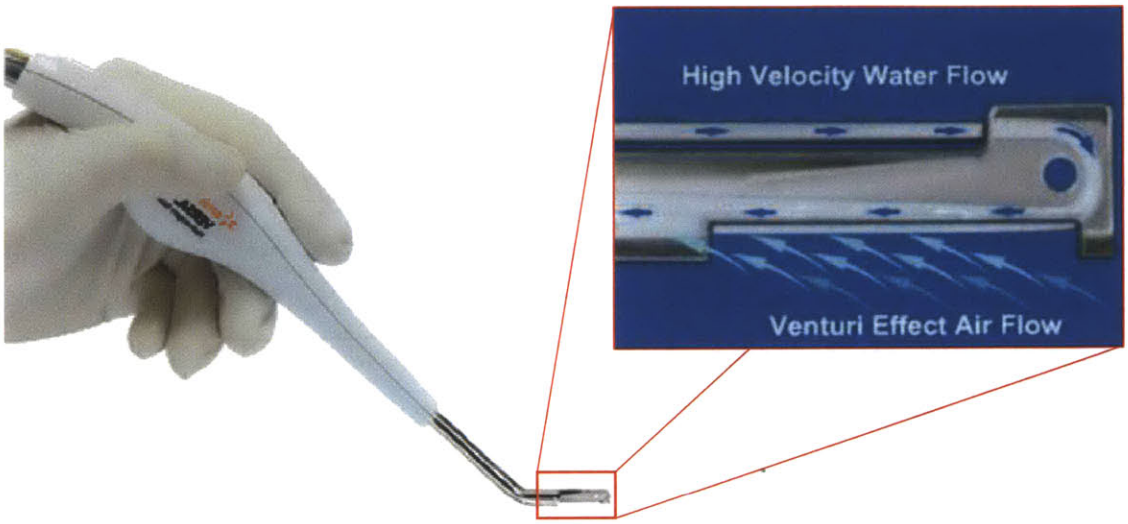

Figure 2-2: The Versajet Hydrosurgery System^{TM} directs a single jet parallel to the wound surface. The venturi effect draws soft tissue into the jet path, where it is cut and evacuated [21]. Figure adapted from [23] and [24].

of injection injuries and jet injection devices suggests that 15 MPa is required to puncture human skin with a liquid jet of diameters between 100 and 500 µm, though this pressure has been shown to increase as jet diameter decreases. Larger loads and greater deformations are required to initiate this crack than to propagate it [25].

Using fracture mechanics to model cuts in deformable bodies gives insight into the mechanisms of crack formation by liquid jet impingement. In a deformable body, a sufficiently sharp tool causes only local deformation. Neglecting friction, cutting with a sharp tool in has been modeled using fracture mechanics as having three modes, shown in Fig. 2-4: (1) deformation, where work from the cutting tool is stored as elastic energy in the deformed body, (2) rupture, where the stored elastic energy irreversibly goes into initiating a fracture, and (3) cutting, where further work from the cutting tool goes into propagating the fracture [26].

Empirical correlations show that the stress necessary to perforate tissue increases with Young's modulus, which one study measured as 0.3 MPa in human skin and 0.5

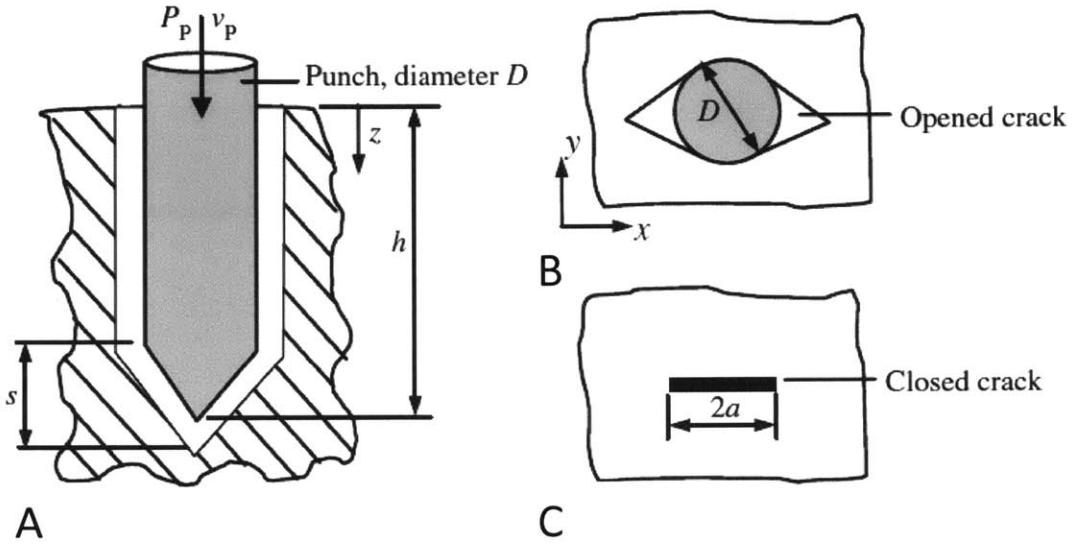

Figure 2-3: Both liquid jets and sharp-tipped punches open a planar crack when they penetrate tissue, as depicted in cross-section in (A) and from above in (B). In (C), the planar crack closes after the punch is removed. Reproduced from [25].

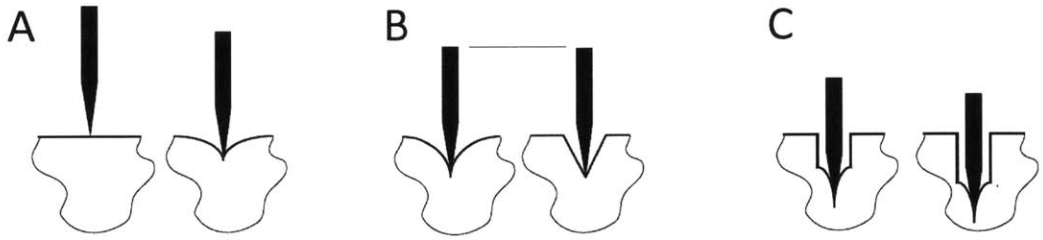

Figure 2-4: An illustration of cutting with a sharp tool in a deformable solid, where a straight segment symbolizes a wall of the original body or a wall created by fracture and a curved segment symbolizes a wall subject to deformation. In (A), a sharp tool causes elastic deformation. In (B), the energy stored in the elastic deformation goes into rupturing the solid, and a fracture is initiated. In (C), the sharp tool deepens the crack through cutting, where energy from the cutting tool goes into propagating the fracture. Adapted from [26].

MPa in porcine abdominal tissue [27]. Tissue stiffness decreases, however, if thermal damage degrades the crystalline structure of the dermal collagen into a gel-like state. Tissue dehydration, by contrast, causes an increase in stiffness [28]. Therefore it is expected that in tissue with degraded collagen, such as sloughy tissue, a lower jet pressure will be needed to penetrate, while dry samples such as eschar will have a higher penetration pressure.

After penetration, the liquid jet slows and stagnates. As Fig. 2-5 illustrates, upon stagnation a bolus of liquid expands spherically outwards from the end of the hole into the surrounding tissue [29]. Thus, less pressure is required to disperse the liquid into the tissue than to bore the hole.

Schramm-Baxter and Mitragori [30] showed that the depth of jet penetration and the width of liquid dispersion both correlate to the power of the jet, given by

$$P_0 = \frac{1}{2}\dot{m}u_0^2, \tag{2.1}$$

where P_0 is the power of the jet at the nozzle exit, $\dot{m}$ is the mass flow rate, and u_0 is the exit velocity. The mass flow rate can be given as

$$\dot{m} = \rho A_0 u_0, \tag{2.2}$$

where ρ is the fluid density and A_0 is the area of the nozzle orifice. Plugging the mass flow rate of Eq. 2.2 into Eq. 2.1 yields the equation for jet power

$$P_0 = \frac{1}{8}\pi\rho D_0^2 u_0^3. \tag{2.3}$$

Experimental data are reproduced in Fig. 2-6 that shows that that both hole depth and the width of dispersion increase with jet power in a logarithmic manner [30].

Lastly, the jet exit velocity can be estimated from the supplied pressure p_{supply} using Bernoulli's equation,

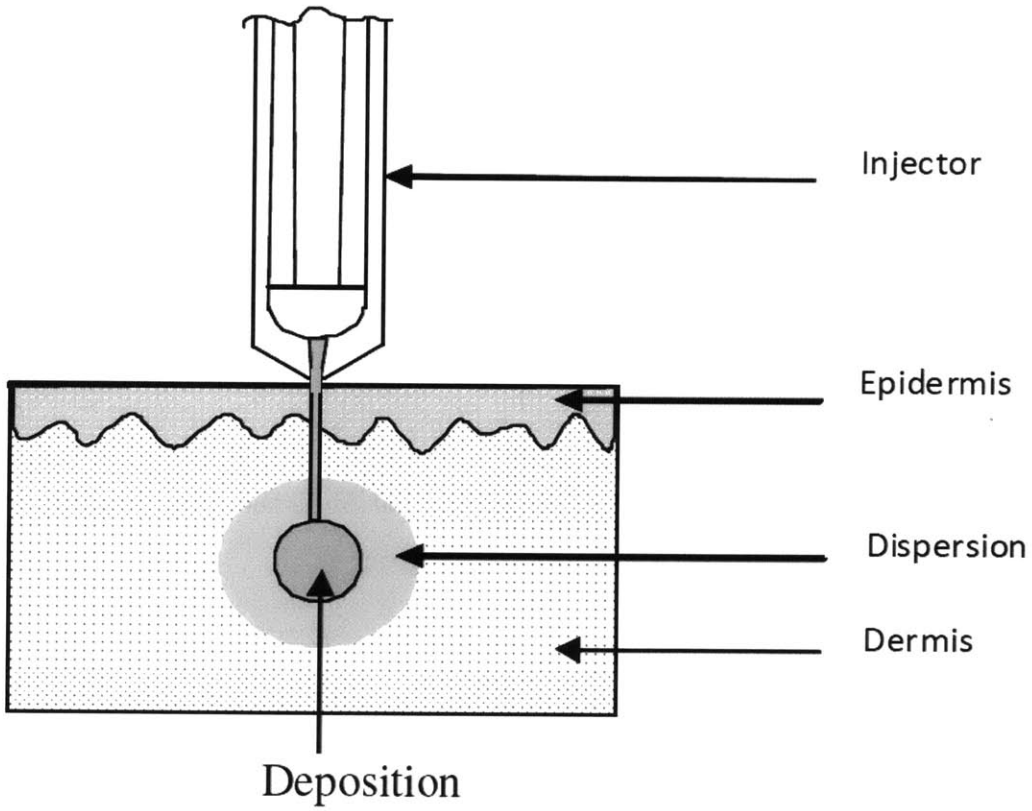

Figure 2-5: During jet injection, the liquid jet slows as it penetrates further into the sample. When the jet stagnates, it expands water spherically outwards into the tissue, as shown above. Reproduced from [29].

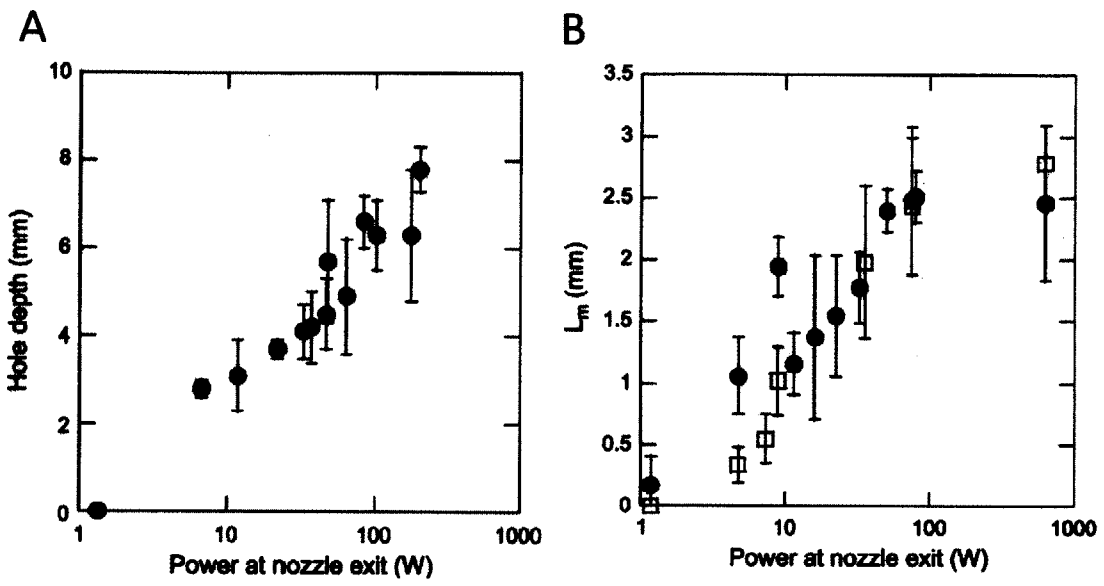

Figure 2-6: Experimental data showing that both the depth of injection and the width of dispersion L_m produced by a liquid jet in tissue scale logarithmically with jet power. Reproduced from [30].

$$u_0 = \sqrt{\frac{2p_{supply}}{\rho}}, \tag{2.4}$$

which in one study was found to predict more accurately than several friction models [31].

2.4 Jet Injection with a Linear Lorentz-Force Actuator

In needle-free injection, a fluid at high pressure is forced through a small orifice, forming a jet. This jet penetrates the skin and delivers the liquid to the tissue. Jet injection driven by a linear Lorentz-force motor gives control of the depth and velocity of the injection. Because the motor is electrically powered, the pressure of the jet is controlled throughout the injection. Internally, the magnetic flux from a central

magnet passes radially outwards through a copper coil (Fig. 2-7). Current through this coil generates Lorentz force that drives the injection [32].

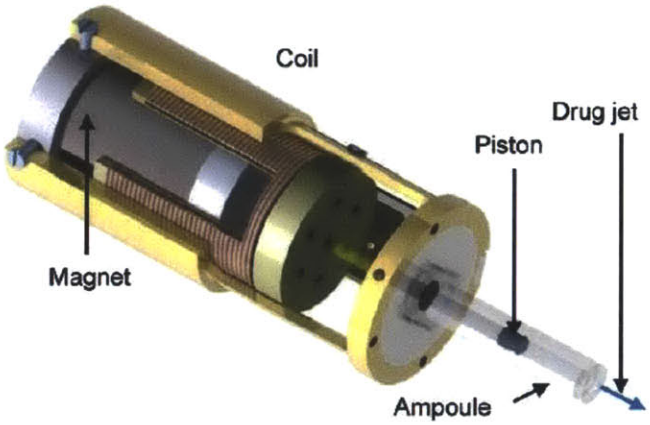

Figure 2-7: A schematic of the MIT Bioinstrumentation Laboratory's needle-free injection device. The coil of the voice coil motor is attached directly to a piston, which forces the drug though a small orifice and into a jet (reproduced from [32]).

By installing multiple actuators in parallel, the motors could continuously supply fluid. In the conceptual drawing shown in Fig. 2-8, two motors alternate in supplying pressurized fluid to a central nozzle, while two more motors apply suction to an outer concentric nozzle. This device shows how Lorentz-force actuators could potentially power a debridement device.

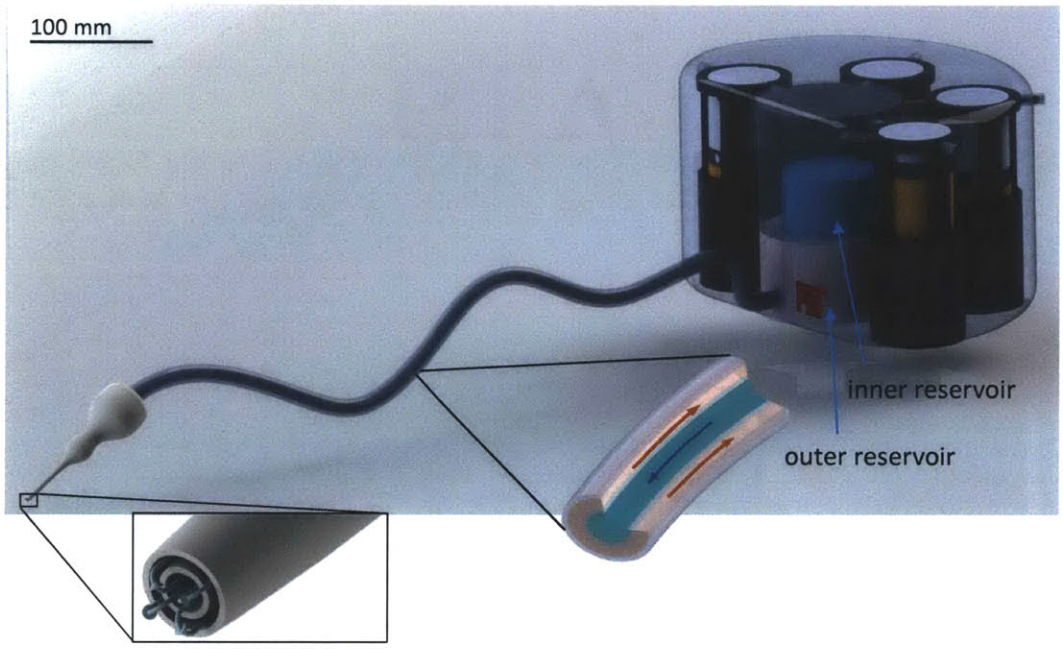

Figure 2-8: A conceptual drawing of a device that uses multiple linear Lorentz-force actuators to supply continuous suction and pressurized liquid to a handpiece.

Chapter 3

Development of Cutting Concept

It was hypothesized that precisely controlled fluid jets could be used to debride a wound. In needle-free injection with a linear Lorentz force actuator, the pressure profile during injection can be tailored to give desired characteristics, such as injecting to a particular depth [32]. By exercising similar control over jets used for debridement, it was conjectured that pressures or pressure profiles could be found that would allow unwanted tissue to be massaged or cut away. This chapter details an exploration of cutting techniques and parameters such as jet pressure, nozzle size, and jet angle and their suitability for debridement.

3.1 Experimental Setup to Supply High Pressure Water

The feasibility of initial cutting concepts were tested using a pneumatic piston pump from Maxpro Technologies [33]. The pump supplied pressures between 2 and 85 MPa and at 20 MPa had a flow rate of 0.011 L/s, comparable to the flow rate used in jet injection (JI).

The output pressure of the piston pump oscillated through a range of about 5 MPa. In testing, the minimum pressure of this oscillation was set to equal the minimum

pressure required to cut; allowing the pressure to dip below this threshold during testing resulted in inconsistent cutting performance. For this reason, throughout this thesis, values given for the supplied pressures refer to the minimum pressure provided.

The auxiliary hardware used to control the water supply is shown in the diagram in Fig. 3-1 as well as the photograph in Fig. 3-2. All tests were performed inside a polycarbonate safety enclosure, and rubber or latex gloves, a face shield, and a lab coat were worn during experiments.

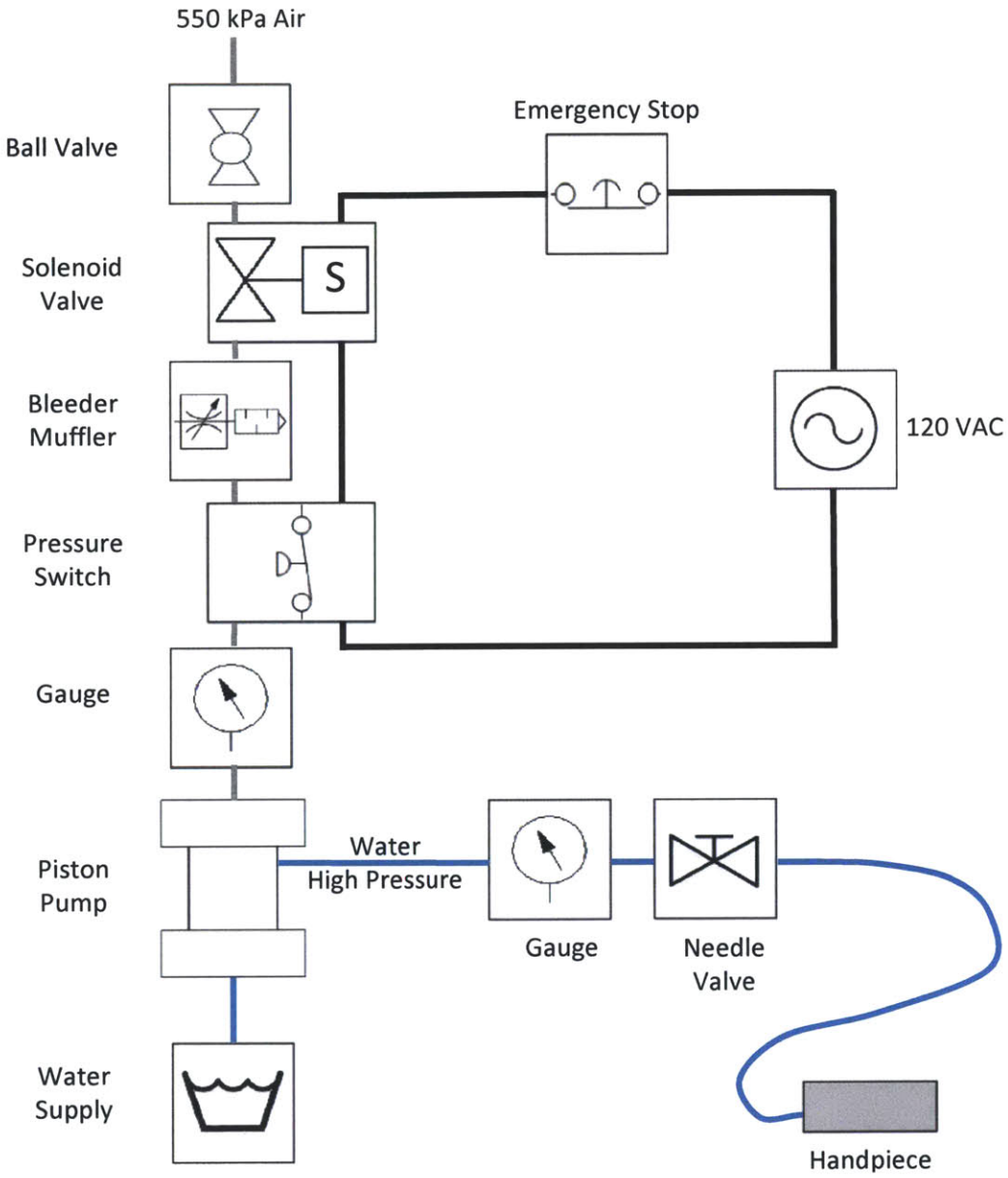

Figure 3-1: Diagram showing setup components. At the input, 550 kPa air is fed through a ball valve to a solenoid valve. On its way to the pump, the air passes through a bleeder muffler, an adjustable pressure switch, and a 400 kPa dial pressure gauge. The air supplied to the pump is controlled coarsely by adjusting the ball valve, and finely by allowing air to bleed out through the bleeder muffler. Both the pressure switch and an emergency stop are able to cut off power to the solenoid valve, causing the valve to close and isolating the pump from the air supply. The pressure switch is set to activate at 700 kPa, higher than the pressure of the compressed air available, yet still less than the 1.4 MPa for which that all the air supply fittings are rated. All connections in the air supply fittings are 1/4 NPT.

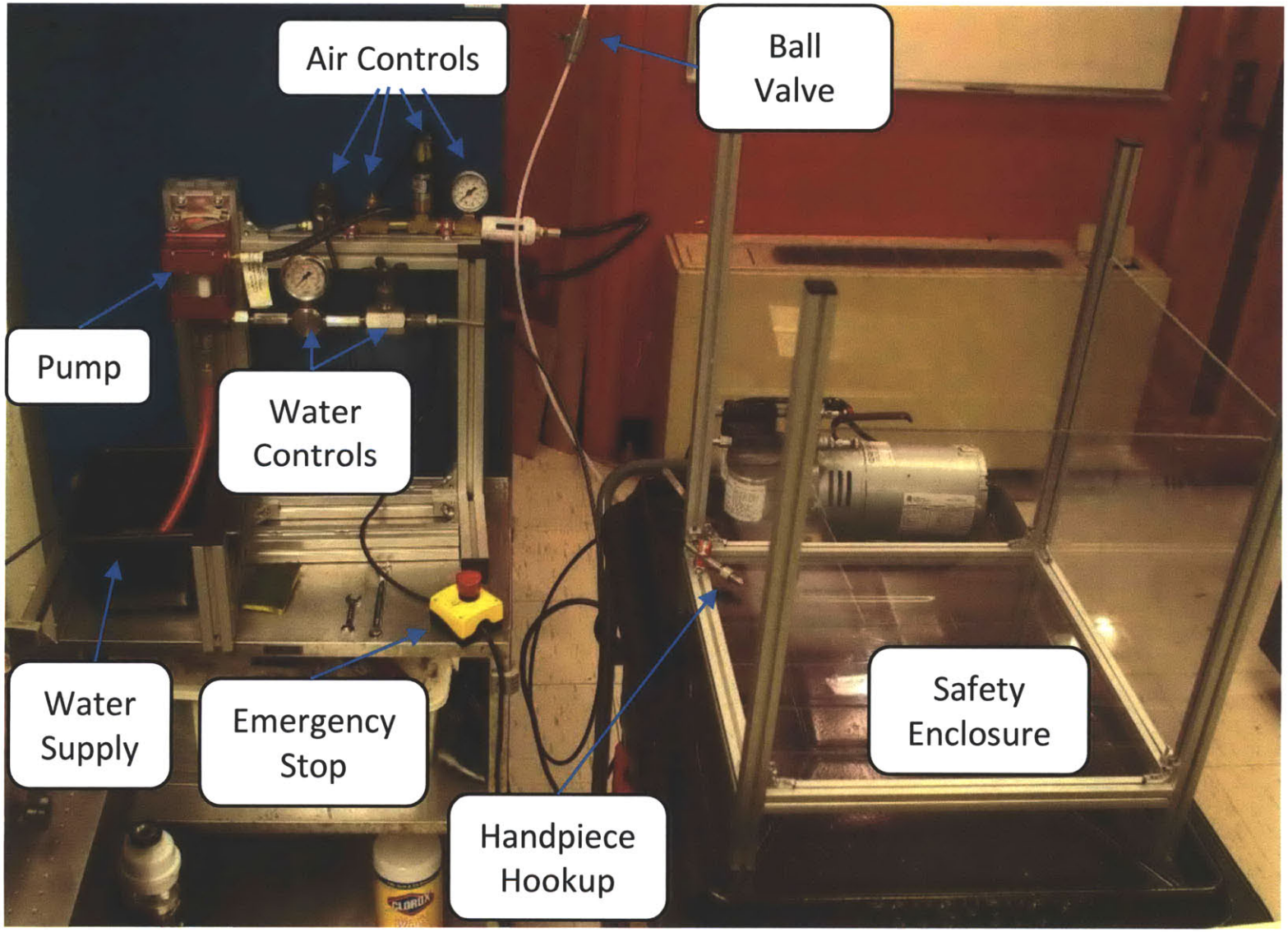

Figure 3-2: A photograph of the setup described in Fig. 3-1.

3.2 Initial Cutting Concepts

The following section presents the progression of debridement jet concepts.

3.2.1 Description of Initial Concepts

Any waterjet-cutting device would need to supply no more water than could be locally removed in order to avoid cross-contamination. The flow rate of an existing lavage device [34] was measured to be 0.018 L/s, and this rate was set as the maximum allowable for new debridement designs.

Initial concepts included a cutting jet that impinged on the wound surface at a slight angle in order to remove more material than the existing hydrosurgical device described in section 2.2. One concept, shown in Fig. 3-3, was based on the idea of a plane or chisel shaving away a thin layer of wood. The water would exit from this device in a wide, flat sheet envisioned to peel back a layer of tissue upon contact with the wound surface. This water sheet would be about as deep as a JI jet, for example 50 to 100 µm, and could be as wide as desired. The water sheet would be formed by forcing water through the narrow slit formed by two half-round rods, so shaped in order to increase the sheet coherence in the narrow dimension. A front retaining plate would hold the half-round rods in place against the outward force of the water pressure.

One difficulty in directing a cutting jet to impact tissue would be to control the cutting depth. Without additional measures, the jet would propagate to a depth dependent on the jet and material characteristics, as described in section 2.3. A low-pressure stream of water was added to the water-sheet design in order to limit the cut depth, as depicted in Fig. 3-4. After peeling back the tissue a certain distance, the cutting sheet would intersect the low-velocity stream. Upon intersection, the cutting jet would dissipate into the low-velocity stream and cut no deeper.

This cutting concept was not experimentally tested because it was estimated to

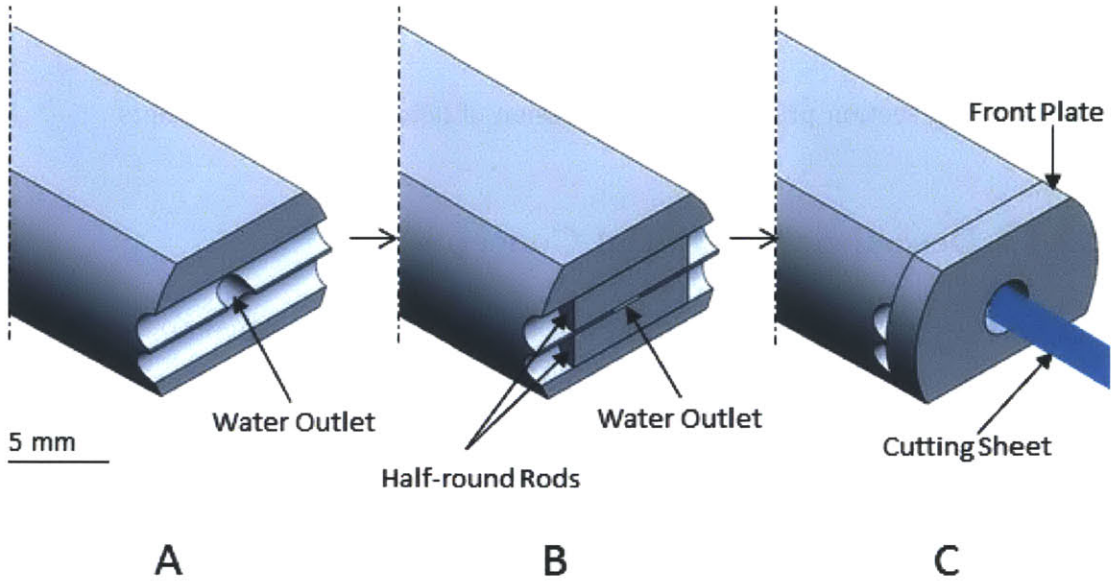

Figure 3-3: A conceptual design for generating a fluid sheet about 100 µm thick. Two half-round rods are held in front of a water outlet by a retaining plate, assembled as shown in the progression A through C. Water forced through these two rods forms the fluid sheet.

have an flow rate greater than the 0.018 L/s limit. A water sheet 100 µm thick and 10 mm wide generated from water pressurized to 15 MPa would have an massive flow rate of 17 L/s, found by plugging velocity from Eq. 2.4 into the equation for volumetric flow rate:

$$Q = A_{jet} u_{jet}, \tag{3.1}$$

where Q is the volumetric flow rate, A_{jet} is the cross-sectional are of the cutting stream, and u_{jet} is the velocity of the cutting stream, and ρ is the fluid density. Adding a low-pressure intersecting stream would further increase the flow rate.

Since generating a cutting sheet used excessive water, the concept was modified to generate a cutting sheet using one or more discrete nozzles. As depicted in Fig. 3-5, these nozzles swivel back and forth in a plane, together sweeping out a cutting plane. If ten swiveling nozzles 100 µm in diameter were used to generate the cutting

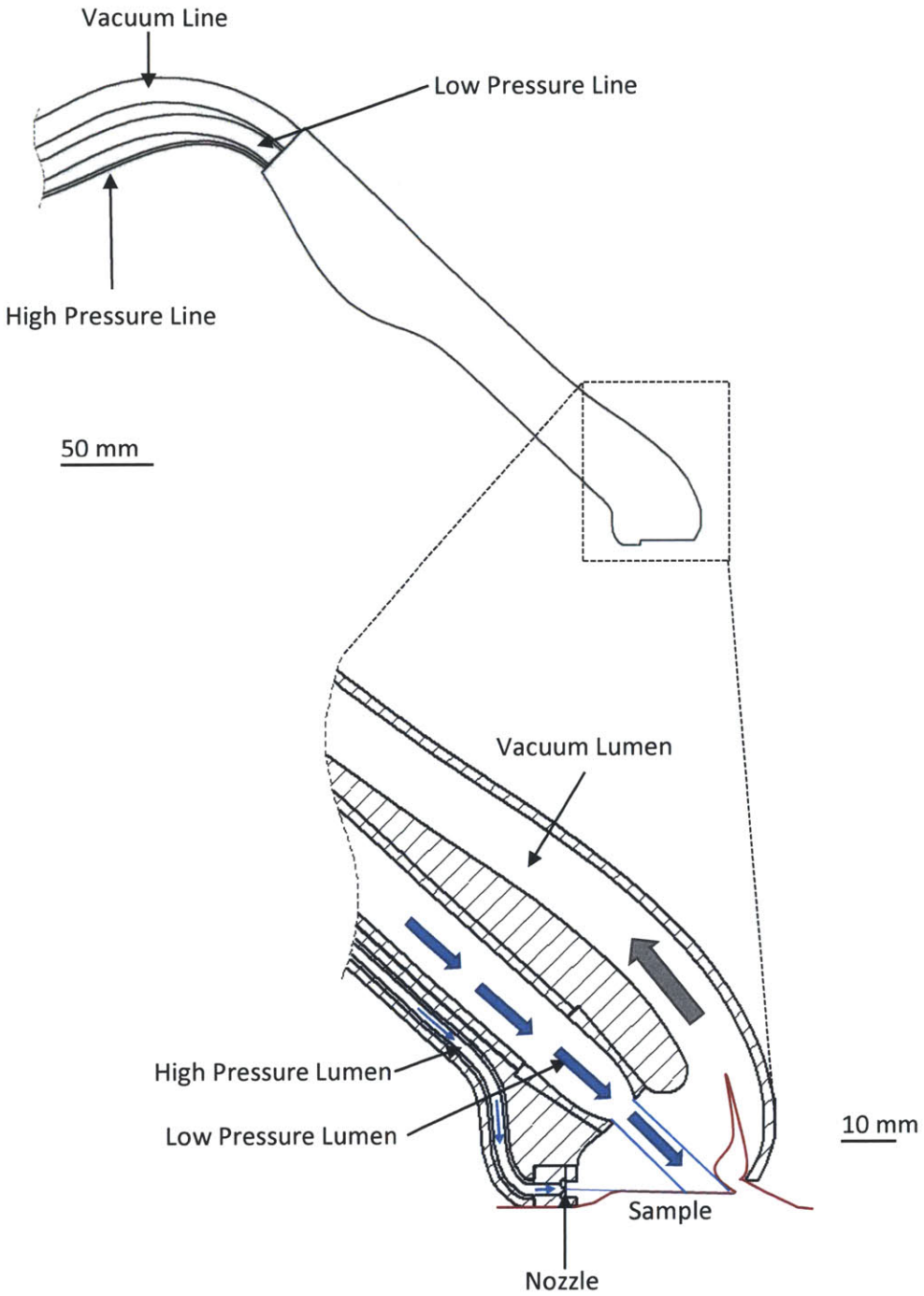

Figure 3-4: A device concept that implements the cutting sheet. Suction draws a portion of the tissue upwards, where it intersects the cutting fluid. A portion of the tissue is separated and drawn into the vacuum lumen. A low pressure fluid stream intersects with the cutting fluid, limiting the depth of penetration.

plane with 15 MPa water, the flow rate would be an acceptable 0.013 L/s.

Figure 3-5: The cutting sheet on the left has an unacceptably high flow rate. On the right, a cutting sheet is generated with discrete swiveling nozzles whose jets sweep back and forth in a plane, creating a cutting sheet with a lower flow rate.

The concept efficacy was assessed using a single handheld nozzle, as described in the following sections.

3.2.2 Experimental Setup

Ceramic nozzles supplied by Small Precision Tools [35] were used to test the feasibility of cutting concepts. These nozzles, shown in Fig. 3-6, have been shown effective for the delivery of needle-free injections through the tympanic membrane (ear drum) [36]. Fig. 3-7 shows a simple wand made to interface between the high-pressure hose and the ceramic nozzle. An M8 threaded cap held the nozzles to the wand. An acrylic crush washer, cut from a 1.4 mm acrylic sheet with a laser cutter, created a watertight seal between the wand and the nozzle base. There was a 50 µm gap between the outer diameter of the crush washer and the inner diameter of the mating cap, small enough that any significant expansion of the crush washer under pressure was constrained by the mating cap.

Five nozzle sizes were tested: 50, 75, 100, 200, and 300 µm. Table 3.1 gives the measured maximum pressure that the pump was able to supply to a single nozzle of each size. The pump is able to supply higher pressures to the smaller nozzles. When a clogged nozzle that allowed no water flow was tested, at a pressure of 48 MPa, the

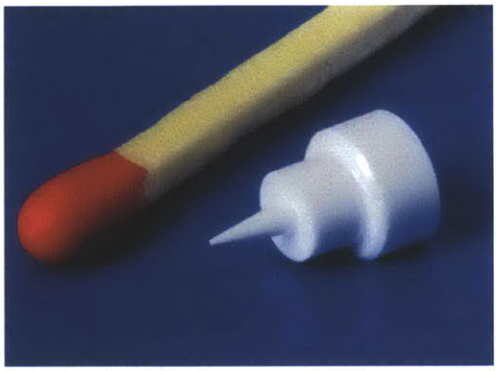

Figure 3-6: A photograph of the type of ceramic nozzle employed, reproduced from SPT [35].

Figure 3-7: The single nozzle debrider wand. On the right are the acrylic crush washers that created a watertight seal between the ceramic nozzle and the debrider base.

tip of the nozzle fractured.

Table 3.1: Maximum pump pressure for each nozzle tested.

Nozzle Dia. (µm)	Pump Max Pressure (MPa)
50	Nozzle Fracture at 48
75	40
100	30
200	10
300	2.5

Nozzle Maintenance The ceramic nozzles were prone to clogging. Occasionally the nozzle would fully clog, allowing no liquid to pass through. More frequently the nozzle would partially clog, outputting a diffuse mist. These clogs frequently occurred when the nozzles were unused for a day or more. The nozzles would also clog during use with particles from the thread sealant tape and other sources. Replacing the thread seal tape in upstream fittings with Loctite 545 thread sealant [37] and installing an in-line 10 µm filter reduced clogging during operation.

A clogged nozzle could, in most cases, be cleared and restored to full functionality using sonication [38] together with VWR Aquasonic Cleaning Solution [39]. Clearing could be enhanced by pre-treatment wit either of two methods: a 50 µm wire could be threaded through a partially-clogged nozzle and wound around around the nozzle walls, an/or an unclogged nozzle could be used to pressure wash the clogged nozzle.

3.3 Simulating a Sloughy Wound

Slough is a stringy mass of devitalized tissue whose color is indicative of the level of bacterial colonization: white for low colonization and yellow or green for higher bacterial counts [40]. Initial debridement concepts were tested on simulated slough because, as the softer of the two types of necrotic tissue, slough was expected to exhibit cutting behavior more similar to healthy tissue (described in Section 2.3).

The compromised structure of slough was mimicked by degrading the extracellular matrix (ECM) of porcine tissue samples with acetic acid. Healthy skin is structurally supported by the dermal ECM, which is primarily composed of collagen in a characteristic triple-helix configuration of three polypeptide chains. Acetic acid is one of the most widely-used solvents for dissolving collagen [41]. Dilute acetic acid causes collagen to swell, unfold, and partly dissolve [42], with exposure to concentrations as low as 0.3% for one hour shown to cause a substantial re-arrangement of intermolecular bonds in rat tail tendons [43]. Higher concentrations of acid burn tissue, causing protein to precipitate and form a dry, hard eschar [44]. Acetic acid at concentrations of 50% or higher produced moderate to severe burns on the skin of guinea pigs [45].

To simulate slough, 10% acetic acid was applied to a sample of post mortem porcine abdominal tissue with the epidermis partially removed by scraping. The acid was pooled on the surface of the sample, which was then sealed and incubated for approximately three hours at 25°C. Afterwards, the sealed sample was stored at 4°C and warmed to 25°C at the time of testing. Treatment with acetic acid fixed the tissue, causing the dermis to become stiff and translucent (Fig. 3-8), in contrast to the supple and opaque pre-treated tissue. As the resulting tissue was moist and had experienced the characteristic breakdown in collagen structure, this treatment with acid successfully mimicked important characteristics of sloughy wounds.

3.4 Experimental Testing of Initial Concepts

The purpose of these first tests was to explore cutting concepts and to develop intuition for cutting behaviors. The behavior of each nozzle size was tested in sloughy tissue throughout the pressure range the pump was able to supply. Table 3.2 shows the maximum pump pressure tested at each nozzle size, as well as the jet power and flow rate at that pressure.

Any jet directed to impinge on the tissue would inject water into the tissue. With

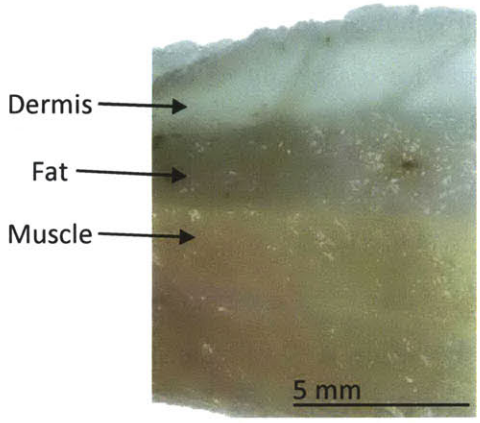

Figure 3-8: A cross-section of tissue after treatment with 10% acetic acid, showing the translucence of the dermis.

Table 3.2: The maximum pump pressure tested for each nozzle size, with the corresponding jet power and flow rate. The jet power is calculated using Eq. 2.1 and the flow rate using Eq. 3.1

Nozzle Dia. (µm)	Pump Pressure (MPa)	Jet Power (W)	Flow Rate (mL/min)
50	40	29	33
75	40	50	75
100	30	58	115
200	10	44	266
300	2.5	13	300

each reduction in nozzle size, water injection because less evident, due to the nozzle's lower flow rate. The depth of cut created, however, also decreased, as predicted by the decreased jet power.

Jets from the 200 and 300 µm nozzles were difficult to direct; the force on the handpiece from the exiting water was noticeable and interfered with pointing the jet as desired. Furthermore, these larger jets exerted global forces on the sample, propelling the entire sample away from the impinging stream.

By contrast, jets from nozzles with orifices 100 µm or smaller were more easily controlled: they exerted local forces on the cut area, and they imposed no noticeable force on the handpiece. Example cuts are shown in Fig. 3-9.

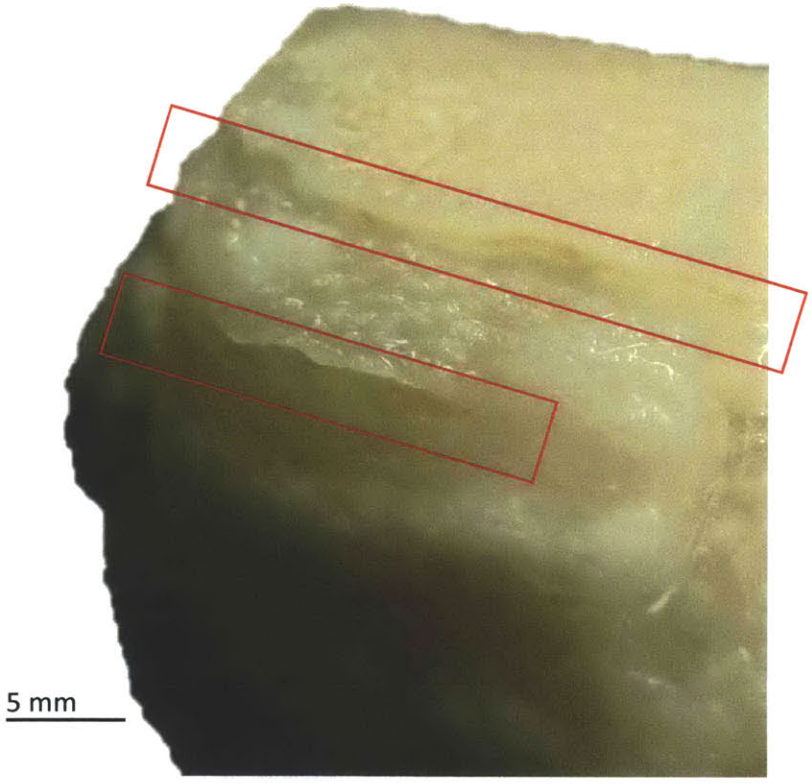

Figure 3-9: The water jet sliced the tissue treated with 10% acetic acid, making cuts that were barely visible unless the two edges were spread open to show the cut depth, as in the picture above. The depth of cut increased with jet power.

In subsequent testing, the 75 µm nozzles were primarily used. They exerted only

local forces, injected less water than the 100 µm nozzles, and cut more deeply and clogged less frequently compared to the 50 µm nozzles.

Fig. 3-10 shows the depth of cut created by the 75 µm nozzle as a function of pressure. These cuts were made with the jet directed to impinge on the surface at a 45 degree angle, in order to mimic the expected angle of a debridement jet. When passes were made at 5 MPa, the tissue would whiten and swell with injected water, but no cut was made. Between 10 MPa and 15 MPa, the cut depth increased as a function of pressure. At 15 MPa jet cut completely through the dermal layer, and further increases in pressure did not result in deeper cuts.

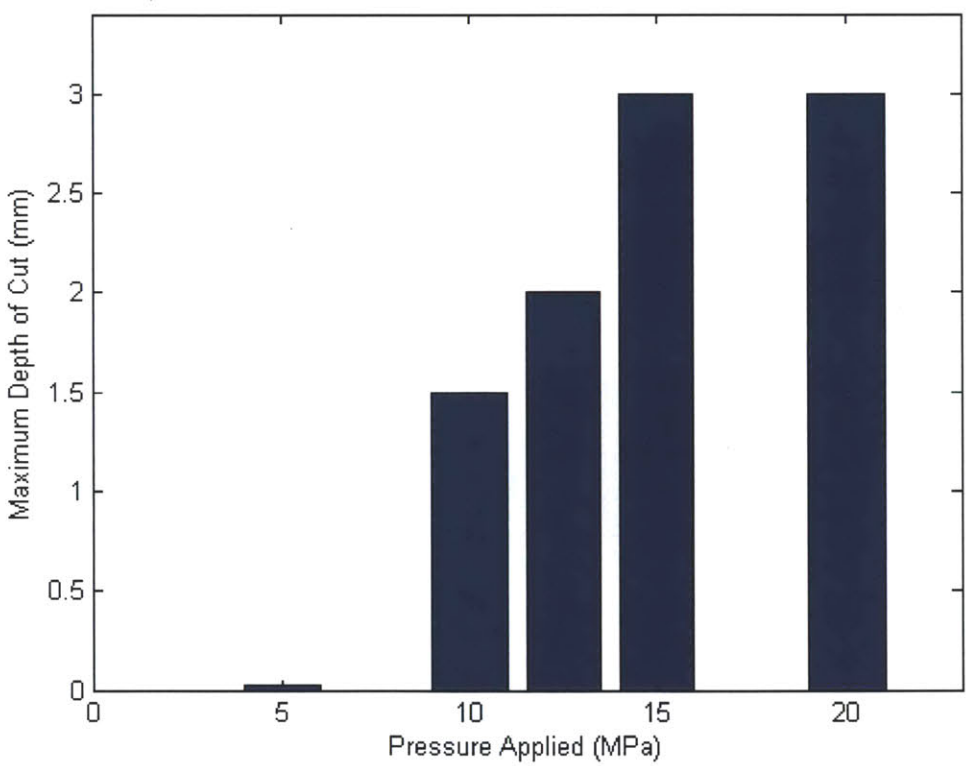

Figure 3-10: Depth of cut made in acid-treated tissue with 75 µm nozzles as a function of pressure. With both 15 and 20 MPa applied, the jet cut through the dermal layer to the underlying fat.

A single angled cut was insufficient to remove material. By making two parallel

cuts, with the second cut angled so that it intersected the first one beneath the surface, it was possible to separate a section of tissue from the sample, see Fig. 3-11. This observation inspired the next generation debridement device, as described in the following chapter.

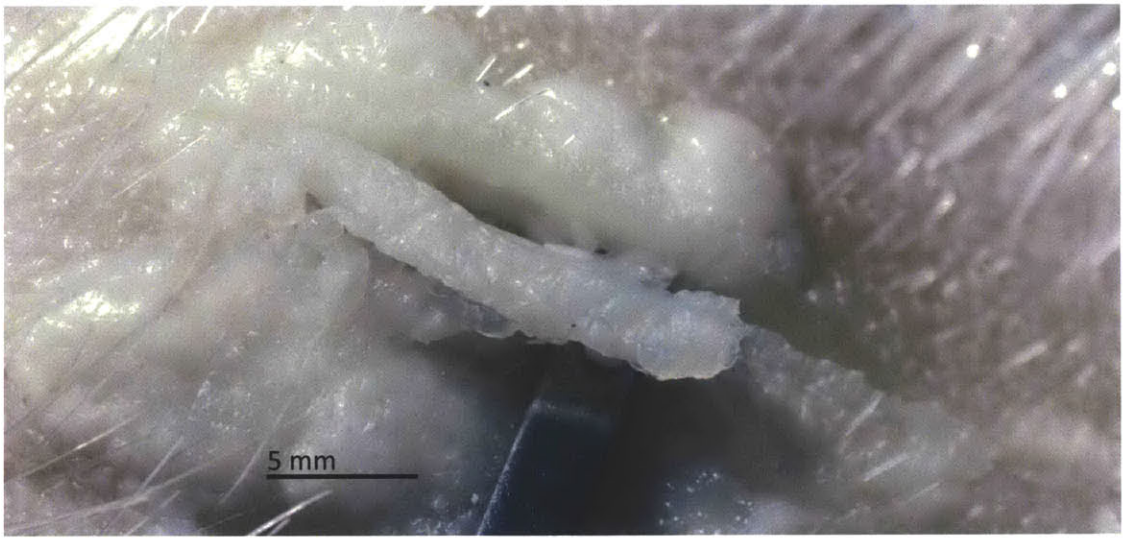

Figure 3-11: By making two sequential cuts, it was possible to excise section of acid-treated tissue, as shown above.

Chapter 4

Dual Nozzle Cutting Instrument

Two parallel cuts made by a single jet were shown in the previous chapter to be able to excise tissue, albeit in a highly path-dependent manner. This chapter describes a debridement device that includes two cutting jets to accomplish the tissue excision in only one motion. As illustrated Fig. 4-1, the two jets make simultaneous parallel cuts. Because the jets are angled to intersect in the subsurface, their motion excises a section of the sample.

4.1 Device Description

Designed for flexibility in testing, the dual-nozzle device allows adjustment in the angle and distance between the two nozzles. With the jets intersecting at 120°, the nozzle tips can be set to between zero and 21 mm apart. With the jets intersection at 90°, the nozzle tips can be set to between 9 and 30 mm apart. Three example configurations are shown in Fig. 4-2.

The nozzle configuration defines the cross section of the excised strip. If the nozzle tips are in contact with the sample surface during a cut, the width of the strip is equal to the distance between the nozzle tips. Fig. 4-3 shows that changing the angle of the nozzles while maintaining the same distance between the tips determines the depth

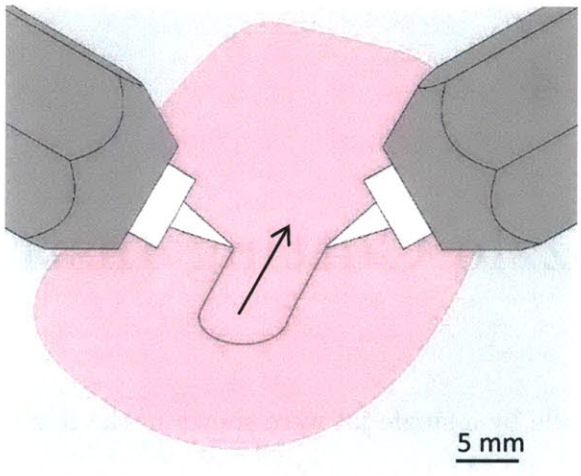

A

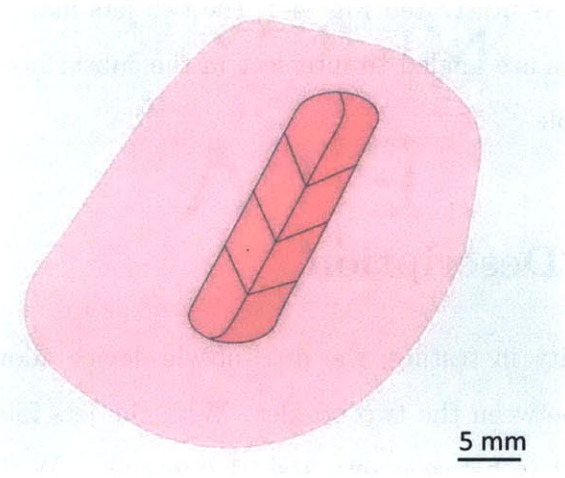

B

Figure 4-1: Method for excising tissue with two nozzles. In (A), the nozzles each simultaneously make a cut. Because the nozzles are angled towards each other, their cuts separate a section of tissue, which has been removed in (B).

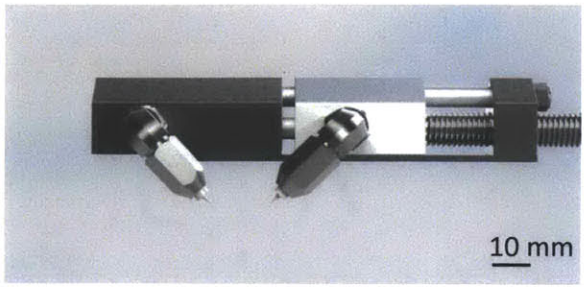

A

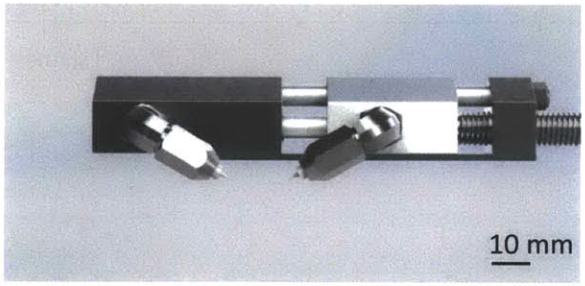

B

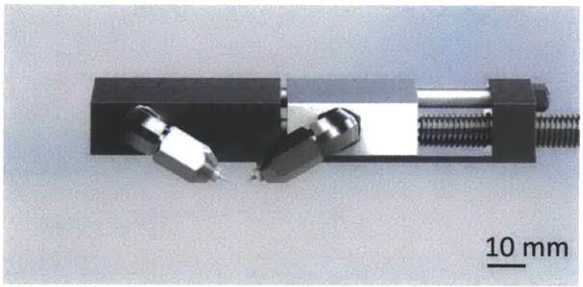

C

Figure 4-2: The two-nozzle device has adjustable angle and distance between the nozzles, with three example configurations shown. In (A), the nozzle tips are 15 mm apart and directed to intersect at 90°. In (B), the nozzle tips are 15 mm apart and directed to intersect at 120°. Finally, in (C), the nozzle tips are 4 mm apart, and they are directed to intersect at 120°.

of cut. In each case, the two nozzles remove a strip triangular in cross-section, and hence the action of the two jets can be succinctly described as a cutting V.

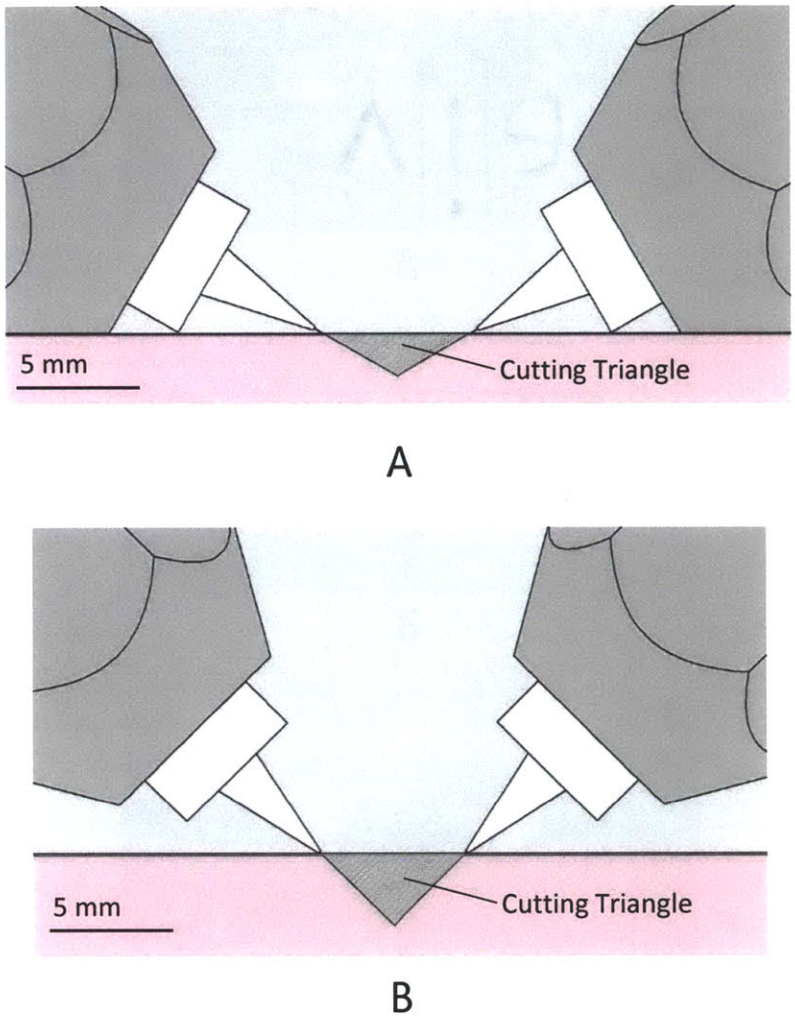

Figure 4-3: Cutting cross-section defined by nozzle distance and angle. 120° and 90° shown.

The base of the device is flat in order to bring the nozzle tips closer to the sample. An external frame, consisting of a base plate and connecting rod, secure the assembly against the force of the internal high-pressure fluid.

Fig. 4-4 shows a section view of the device. The nozzles are mounted onto

stainless steel Yor-Lok elbow fittings referred to as nozzle arms. Sandwiched between the elbow and the nozzle is an acrylic crush washer and a double ferrule, which are made watertight through the compressing action of a threaded cap. The nozzles, ferrules and threaded cap are shown in Fig. 4-5.

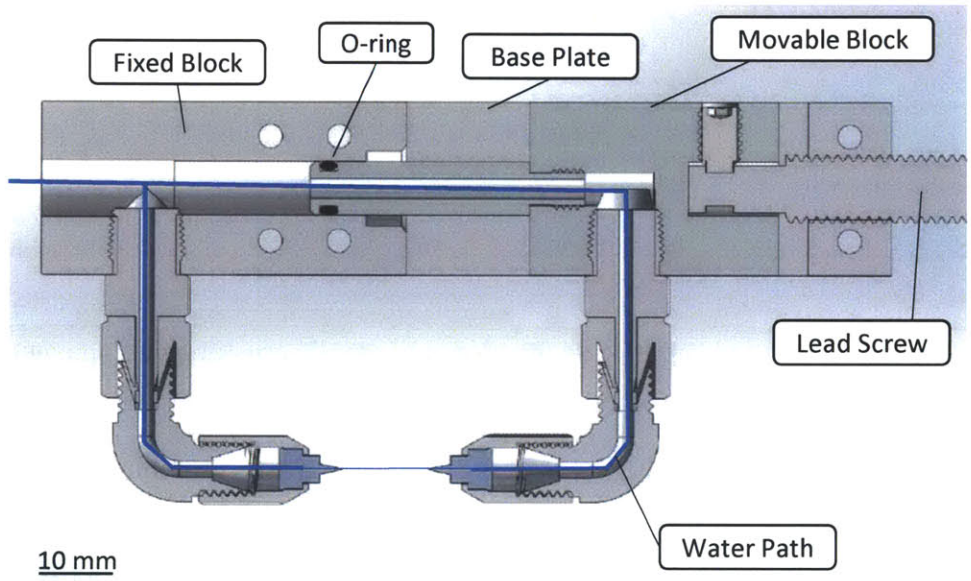

Figure 4-4: A cross-section of the cutting device showing the water path.

Each elbow clamps onto a 3.175 mm tube stem, which in turn mounts into a metal block with a 1/8 NPT thread. When the nozzle arms are rotated, this elbow rotates around the tube stem without losing the watertight seal.

One nozzle arm was mounted in a 304 stainless steel block that was rigidly fixed to the frame. The other was mounted in a movable 6061 aluminum block. The moveable block engaged with a lead screw via an extended point set screw. Turning the lead screw caused the movable block to translate and adjusted the distance between the nozzle tips.

A 6061 aluminum pipe extended between the two blocks, creating a fluid con-

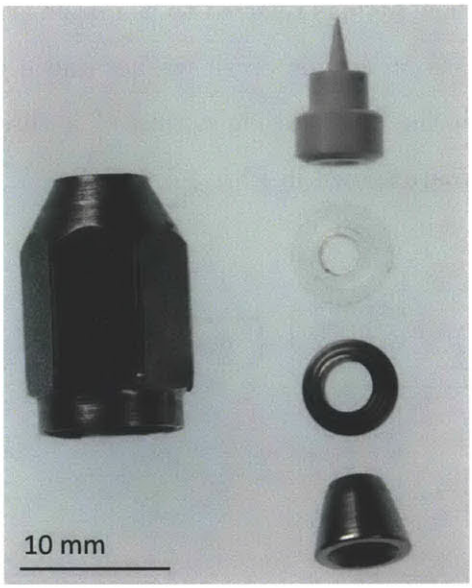

Figure 4-5: The threaded cap, nozzle ferrules, and acrylic crush washer that mounted the nozzle to the nozzle arm.

nection. The pipe, shown in Fig. 4-6, was threaded into the aluminum block using an M4 thread and sealed with Loctite thread sealant [37]. A male O-ring created a movable watertight seal between the pipe and the fixed block. Because the aluminum pipe was made of a softer material than the stainless steel fixed block, particulates in the fluid channel would preferentially embed in the pipe and leave a smooth sliding surface in the fixed-block channel.

A rendering of the two-nozzle handpiece is shown in Fig. 4-7.

Figure 4-6: The pipe that allowed fluid communication between the two nozzle blocks, with the O-ring installed.

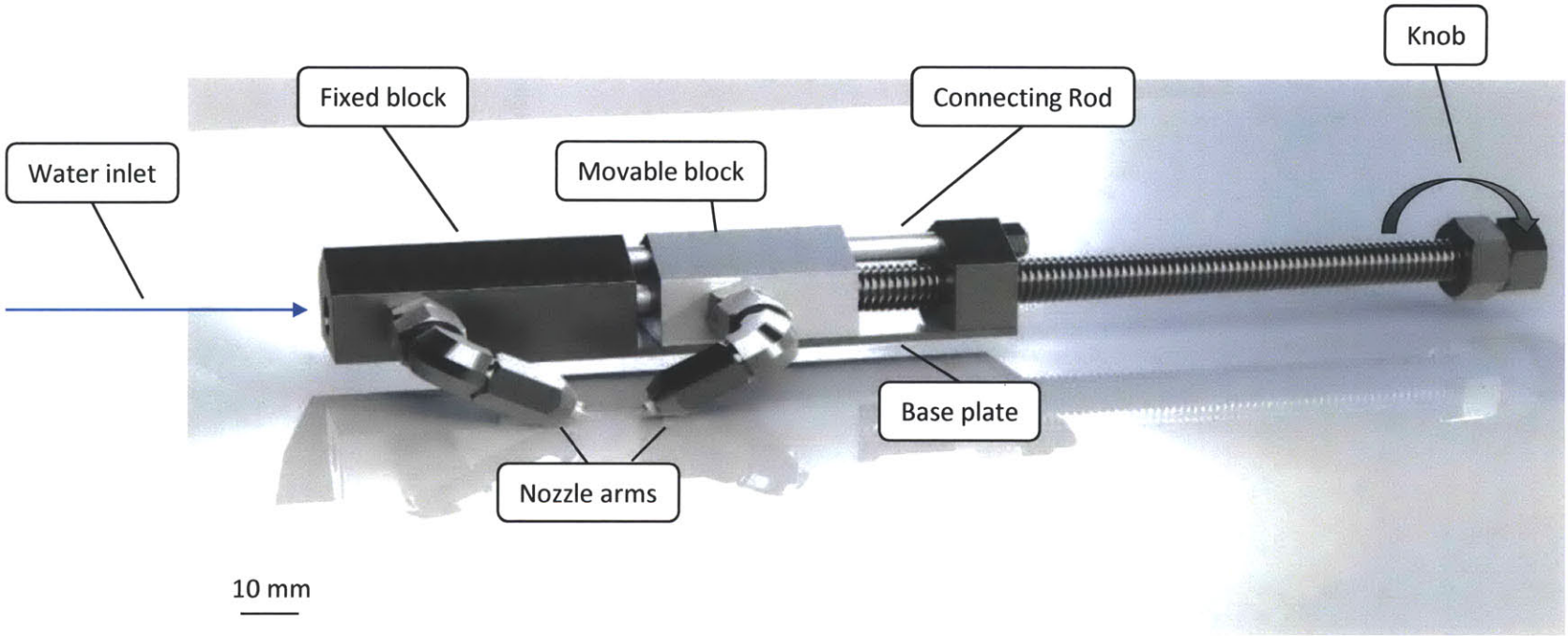

Figure 4-7: Each nozzle is mounted in a nozzle arm that can swivel, thus changing the angle of the jets. The two arms are mounted in separate metal blocks. A knob controls the relative distance between the blocks. By swiveling the nozzle arms and turning the knob, the angle and distance between the nozzles can be adjusted.

4.2 Cutting with Two Nozzles in a Tissue Analog

The first tests of the dual-nozzle device were performed using a tissue analog, 10% acrylamide poured into 55 mm petri dishes. The clear acrylamide offers the advantage of making visible the subsurface behavior, and the substance has been employed in studies of needle-free jet injection [30]. A minimum pressure of 2 MPa was required to cut the acrylamide.

In the initial tests, the jets were arranged so that one would cut just behind the other as the nozzles were moved along the sample; they missed intersecting each other by less than a millimeter. The two jets would separate a length of sample with a triangular cross-section. This separated section was visible, however, only by observing the subsurface cutting pattern: the surface adhesion between this section and the remainder of the sample was large enough that the section could not be removed without damaging the sample. Furthermore, the subsurface patterns showed that the cuts penetrated deeper than the triangular section, creating an x-shaped pattern in the sample.

When the jets were arranged to exactly intersect, they dissipated into a fine mist, demonstrating the effect of impinging jet atomization. In impinging jet atomization, two high-energy jets of equal size collide to form a liquid sheet perpendicular to the plane containing the two jets. The jets are entirely dissipated into droplets shed from this sheet, with the exact behavior dependent on the impingement angle, jet velocity, nozzle geometry, and fluid density and surface tension. As shown in Fig. 4-8, when the jets collide at a 90° angle, the mist is directed upwards, in alignment with the vector sum of the momentum from the two jets. When the jets collide at 120°, the mist is more diffuse, which correlates to the momentum from the two colliding jets largely canceling each other out. If the two jets collided at 180°, their momentum would exactly cancel, and the mist would not move preferentially in any direction, instead forming a circular liquid sheet [46].

The process of atomization dispelled much of the energy of the cutting jets. In

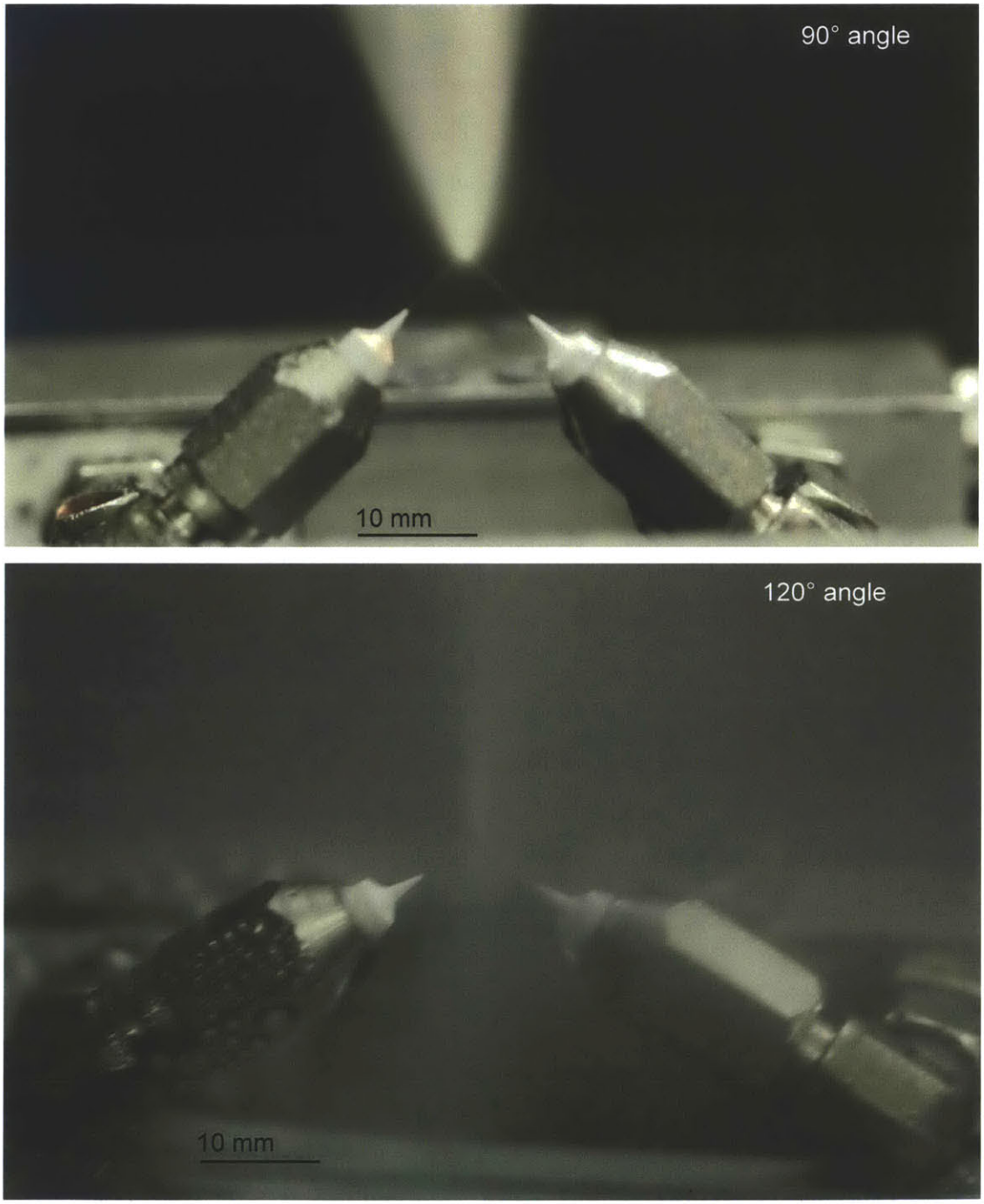

Figure 4-8: Atomization created by impinging jets. The shape of the mist plume corresponds to the net momentum of the mist after the jets collide. The jets intersecting at 90° have a net upward momentum, directing the plume vertically. The jets intersecting at 120° have smaller net vertical momentum, resulting in a more diffuse plume.

one study, three atomizers were shown to dissipate between 85% and 98% of the input energy into thermal energy [47]. For this reason, cuts made in the acrylamide with the impinging jets no longer penetrated deeper than desired. The mist created at the jet intersection did not retain enough energy to cut. Each jet formed an edge of a cutting triangle that terminated at the jet intersection.

With the cut surfaces lubricated by water from the mist, the excised sections were either cleared during treatment, as in Fig. 4-9, or were easily removed with thumb forceps afterward.

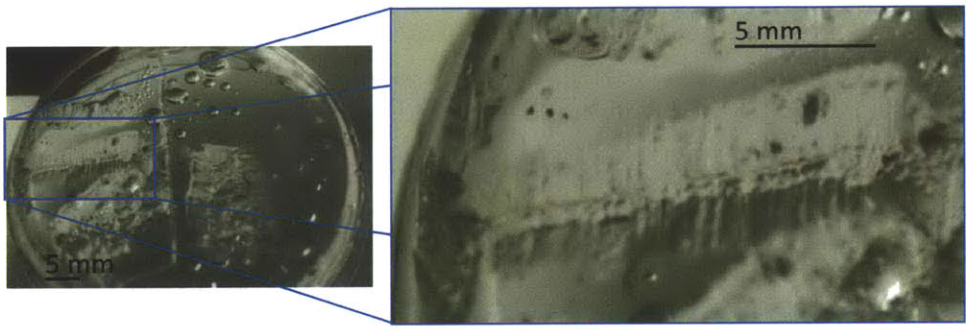

Figure 4-9: A v-shaped cut that penetrated no deeper than the jet intersection, made with 75 µm nozzles spaced 5 mm apart with jets intersecting at 120°.

The limited depth of cut with the impinging jet configuration gave the operator the ability to carve out arbitrary shapes in the acrylamide. The trough shown in Fig. 4-10 was enlarged bit by bit by engaging just the tip of the cutting triangle during each motion. For these cuts, 50 µm nozzles were arranged to intersect at 90°, and the nozzle tips were 10 mm apart. Although it was possible to carve out a general bowl shape, the sides of the bowl were jagged, a relic of the steep intersection angle of the cutting jets.

The top layer of acrylamide could be removed by making a series of side-by-side cuts. The appearance of the resulting surface was dependent on the jet intersection angle used when making the cuts, shown for three configurations in Fig. 4-11. In each configuration, the parallel cuts result in a series peaks and valleys with the peak rising 2 mm above the valley. For the shallowest intersection angle of 85°, the peaks

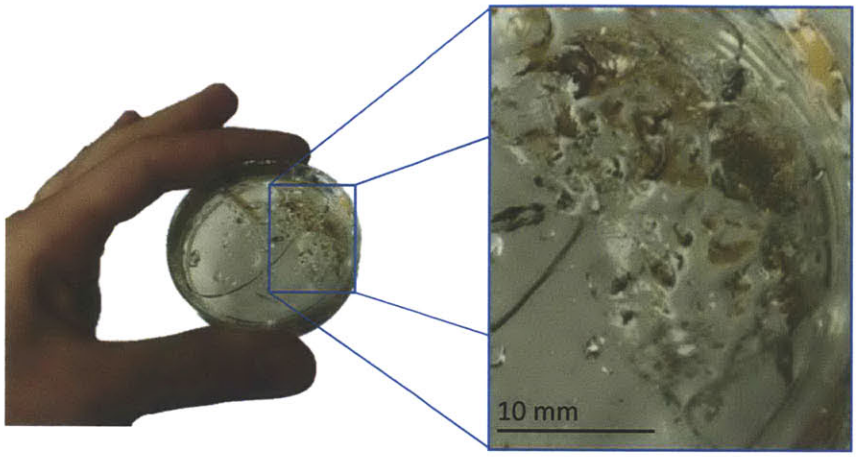

Figure 4-10: A rough surface created in many motions by two jets intersecting at 90° intersection and created by 50 µm nozzles spaced 10 mm apart.

and valleys rise and fall steeply, with only a 2 mm spacing between peaks. For an intersection angle of 110°, the slope is more gradual, and the peaks are spaced every 4 mm. By widening the intersection angle to 130° and making extra smoothing passes, the distance between the peaks was extended to 8 mm. Testing would be required in order to assess the effect of an uneven surfaces such as these on wound healing.

In summary, the two-nozzle technique permitted both controlled cutting in a tissue analogue; the result was a textured surface whose shape depended on nozzle position and angle.

4.3 Cutting Necrotic Tissue

In the previous section, testing of the two-nozzle device in acrylamide showed the importance of aligning the jets to impinge. This section describes the behavior of these impinging jets in cutting necrotic tissue, both hard eschar and moist slough.

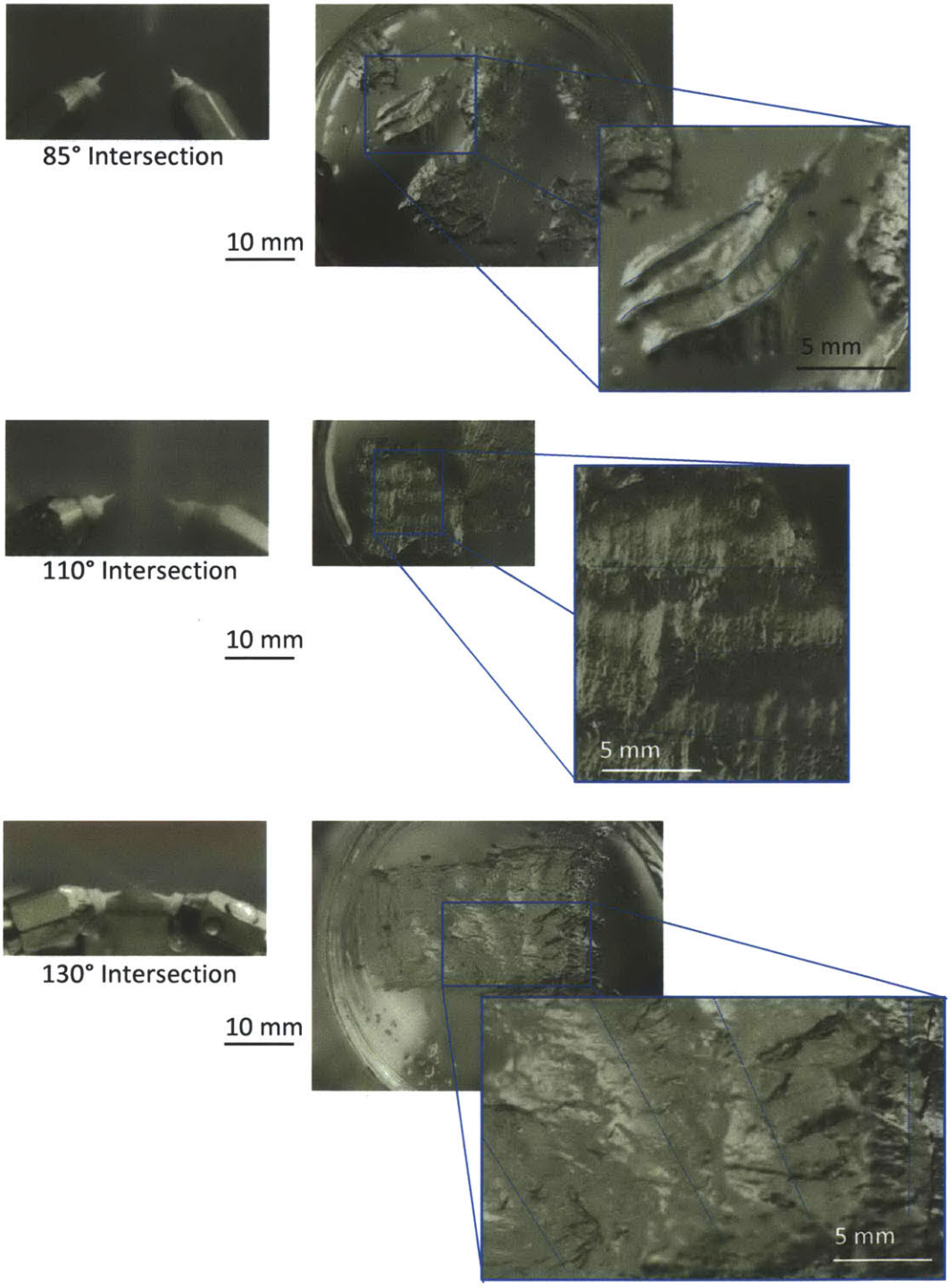

Figure 4-11: Acrylamide testing, 2 MPa jet pressure. A: 85° intersection, tips 10 mm apart. 2 mm between peaks, 2 mm depth. B: 110° intersection, tips 6 mm apart. 4 mm between peaks, 2 mm depth. C: 130° intersection, tips 5 mm apart. 8 mm between peaks, 2 mm depth.

4.3.1 Simulating and Cutting Hard Eschar

Hard eschar is a scab of dry devitalized tissue, frequently present on the heals of patients with restricted blood flow. The mass may be removed surgically or softened with moist dressings for manual removal [40], but other existing debridement devices such as the Versajet^{TM} are unable to remove hard eschar [20].

In order to assess the feasibility of using the two-nozzle device debride eschar, it was necessary to simulate this wound material. Two methods found in the literature were tested. The first method was to scorch the surface of the sample with a butane torch. This method was based on a technique that uses diathermy to simulate eschar on porcine tissue for the purpose of training surgeons [48]. In practice, the butane torch caused carbonization on the surface of the sample, but the sample underneath the carbonization was rubbery, not hard like eschar. This method of simulating eschar was thus rejected.

The second method involved the use of dried dermal tissue as simulated eschar [49]. Four types of samples were dried, shown in Fig. 4-12: untreated porcine tissue, porcine tissue with the epidermis partially scraped away, acid-treated tissue, and a sample of the scorched tissue, as well as a scorched sample already subjected to the debridement jets. After seven days of exposure to air in a fume hood, only the uncut scorched sample was fully desiccated; the drying process had been accelerated due to the moisture removed during scorching. The sample with the intact epidermis was protected from desiccation on all but the edges, and the remaining samples had pockets of moist tissue. The fully desiccated sample was selected as the best eschar approximation.

More energy was required to cut this hard material, and so the nozzles were held at the sample surface, the tip distance was reduced to 2 mm, and the cutting pressure was raised to 15 MPa. This pressure was the same pressure that had made the deepest cuts in sloughy tissue, see Fig. 3-10. The jets were set to intersect at 120° because shallower intersection angles had given smoother surfaces in acrylamide.

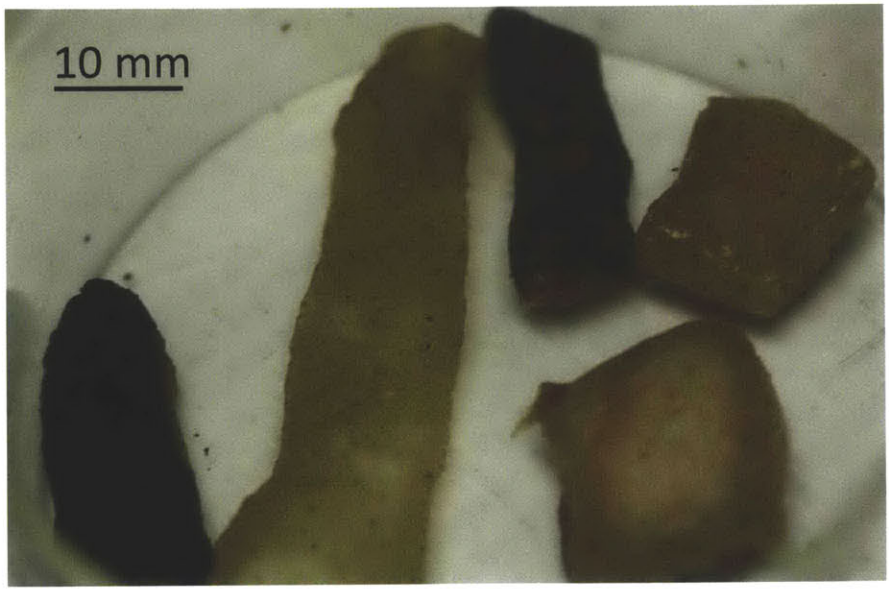

Figure 4-12: Four types of samples were dried in order to simulate hard eschar. Clockwise from left: sample scorched by butane torch, sample treated with acid, sample scorched with butane torch and carbonization rinsed away, sample with epidermis scraped away, and sample with epidermis intact.

Before cutting the sample, the mist created by the impinging jets acted as a lavage and washed away the external carbonization, revealing a deep red surface, shown in Fig. 4-13. Lowering the cutting triangle into the sample, the jets were able to penetrate. No water was injected into this fully-desiccated sample; instead, the water from the jets was reflected at the cut bottom and exited the site in a low-pressure stream. This stream, when reflected vertically, attained a height of about 30 mm.

Because the sample was rigid and did not swell with injected water, it was possible to make cuts with precise control. The second panel of Fig. 4-13 shows a single cut that was made, successfully excising part of the sample. Following that initial cut, the remainder of the sample was debrided in a single continuous operation involving a series of passes. Because the debrided area was a white color and because of the control given with this rigid sample, it was possible to both know where cuts needed to be made and to execute them accurately.

A single pass with the device was sufficient to cut away top impenetrable layer,

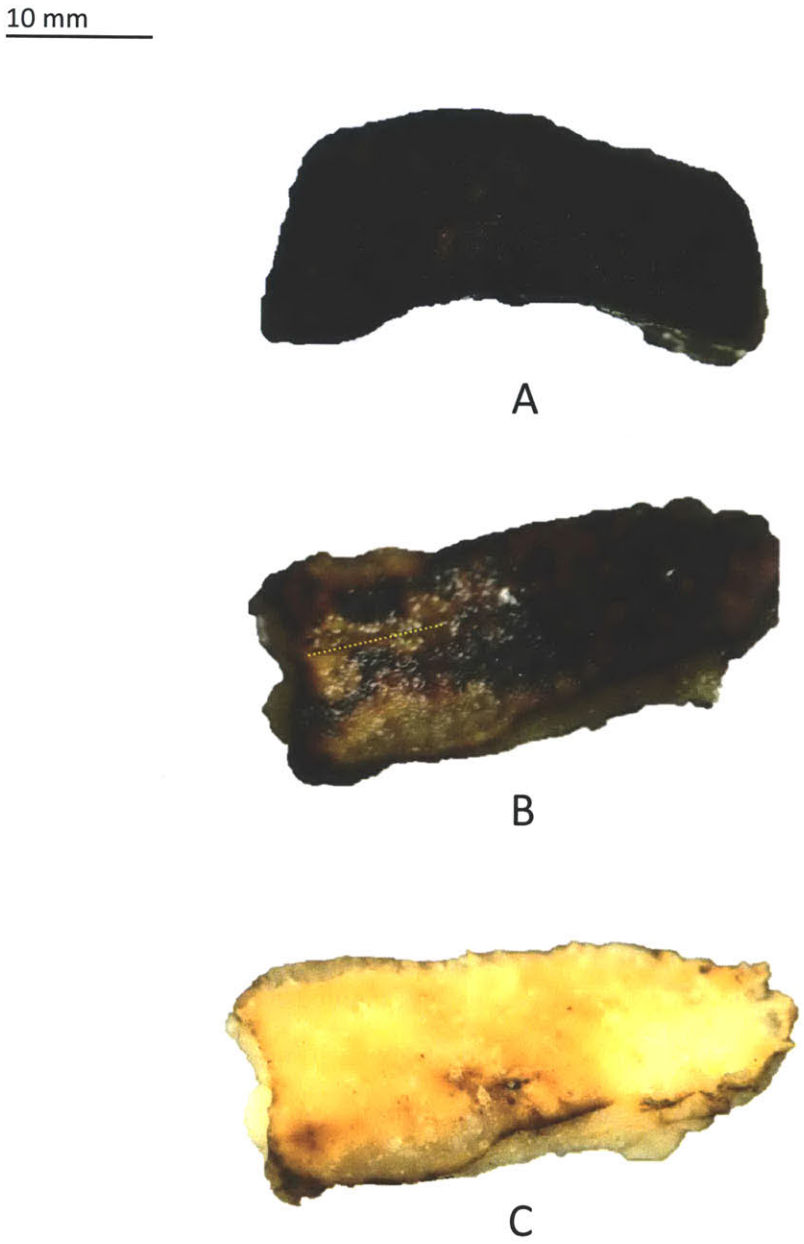

Figure 4-13: The scorched and dried sample (A) before treatment, (B) after lavage and a single cut (traced in yellow dots), and (C) after full debridement.

leaving softened layer underneath. The softened layer could be removed with a curette. Attempting to remove a second layer of material with the jets was successful, though less precise without the advantage of a color change marking the debrided area. Because eschar in chronic wounds is composed of a hardened layer that covers soft tissue, any cuts made with this device that penetrated into the soft tissue layer would inject water into the tissue. To avoid this possibility, the suggested method for using this device in eschar would be to remove the bulk of the eschar with the cutting jets, and then curette the remainder of the softened eschar before the jets penetrate deeply enough to inject water into the underlying tissue. The jets rehydrate the underlying dry tissue, similar to the action of moist dressings. This proposed method could potentially be a time-saving alternative to applying moist dressings, but verification from further tests on samples that include both eschar and soft tissue components will be necessary.

4.3.2 Cutting Sloughy Wounds

As described in Section 3.3, sloughy wounds can be simulated using acetic acid. A pressure of 15 MPa was again used to cut, though the jets cut more deeply in the softer material compared to hard eschar. For this reason, the distance between nozzle tips was increased to 4 mm while the intersection angle was maintained at 120° in order to produce the smoothest surface possible. Again, the nozzle tips were held directly at the tissue surface.

If cuts were made with the nozzle tips closer than 4 mm, the excess energy of the cutting jets would inject water into the dermis adjacent to the cut, causing it to pucker and turn white, as shown in Fig. 4-14. If cuts were made with the nozzle tips spaced at 6 mm, the jets would not cut deep enough to intersect.

Assessing Cut Width and Depth The dimensions of cuts made in sloughy tissue were measured from a 3D model made of the sample surface. To construct this model,

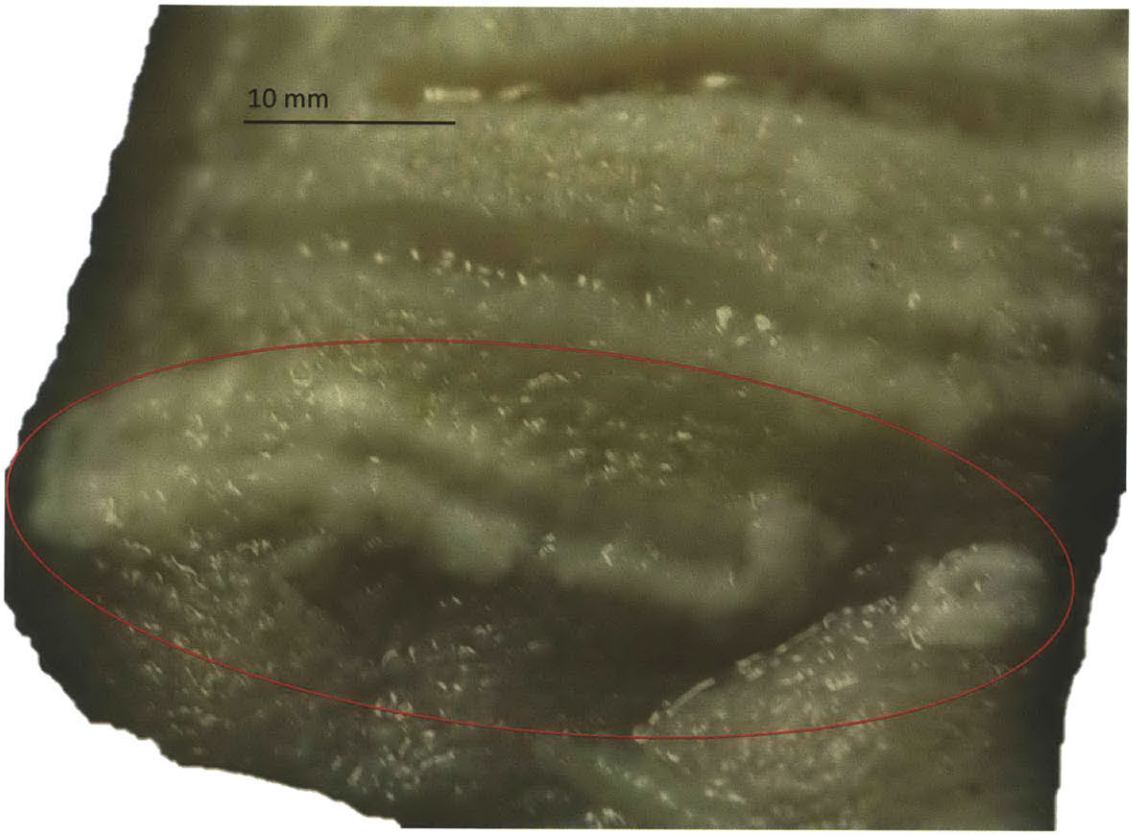

Figure 4-14: With the nozzle tips too narrow, white puckering was observed along the cut. Circled in photo: 15 MPa applied to nozzles with tips 3 mm apart, 75 µm nozzles.

a series of between seven and twenty images were taken of the sample, each image showing from a different angle the cut and an adjacent set of calipers. Before taking photos, the cut and sample were speckled with black spray paint in order to increase the fidelity of the 3D rendering. Software generated a 3D model from these images [50]. Three sets of points of at least fifty points each were manually picked in this model, two sets marking the cut edges and one marking the deepest part of the cut [51]. These points were analyzed in MATLAB to give cut width and depth [52]. These cut dimensions were validated by comparing them to caliper measurements, see Fig. 4-15. This modeling process is shown pictorially in Fig. 4-16.

A tissue sample in which five cuts were made is shown in Fig. 4-17. These cuts have no whitening or puckering, showing that the jets no longer carry excess energy and water is not injected along the cut edges. The cuts made in soft tissue maintain a discernable V-shape, similar to the cutting behavior in acrylamide. The graph at the bottom of Fig. 4-17 gives the cut dimensions made by measuring the width at the top of the V, and the depth from the sample surface to the deepest point of the cut, as discussed above. The graph gives measurements along the length of the cut, following the translation of the cutting V. The average width and depth for each of these five cuts with the standard deviations are shown in Fig. 4-18.

Although there was no whitening at the surface layer and the jets cut no deeper than the intersection point, swelling indicated that water was injected deeper into the sample. This swelling in one part of the sample caused a bulge that visibly distorted the one of the cut dimensions. The cut marked Cut 1 in Fig. 4-17 grows wider as it passes over the area most swollen by deep water injection. At the sample center, Cut 3 was made first. The injected water from the adjacent cuts on either side swelled the tissue and pushed the sides of Cut 3 inwards, making the cut appear narrower and deeper. In future testing, measurements were taken after each cut in order to avoid such distortions. Because water injection caused the shape of the tissue during cuts, it was not possible to control the cut path well enough to make side-by-side cuts.

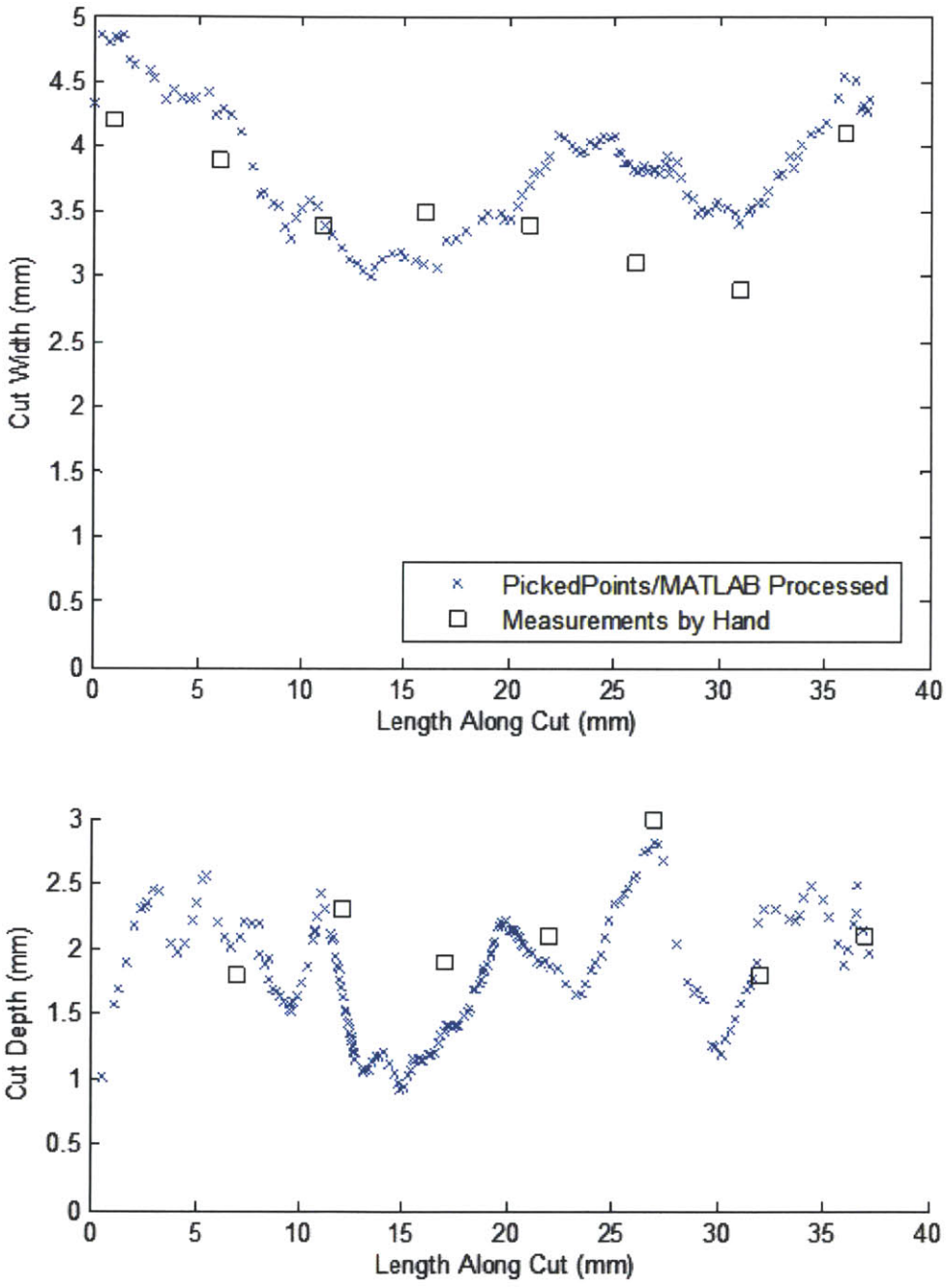

Figure 4-15: Measurements of the cut made with calipers and from the 3D image showed adequate correlation to validate the measurements taken from the 3D model.

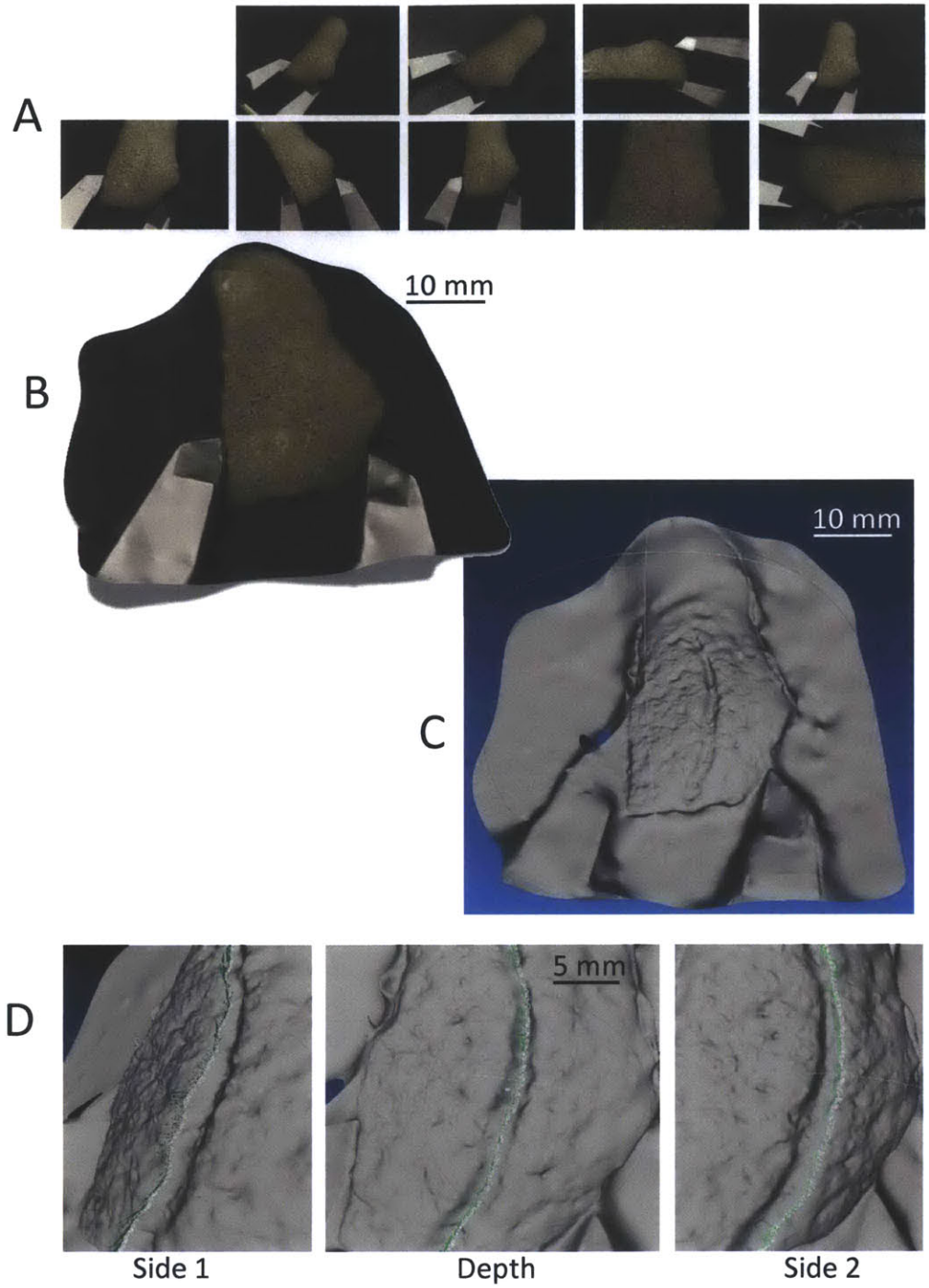

Figure 4-16: To construct 3D images of the cut surface, a series of photos of the cut (A) was uploaded to Autodesk 123D Catch. The STL file from Autodesk's rendering (B) was imported into Meshlab (C), where points were manually designated to mark the cut edges and depth (D). These points were analyzed in MATLAB to find cut width and depth.

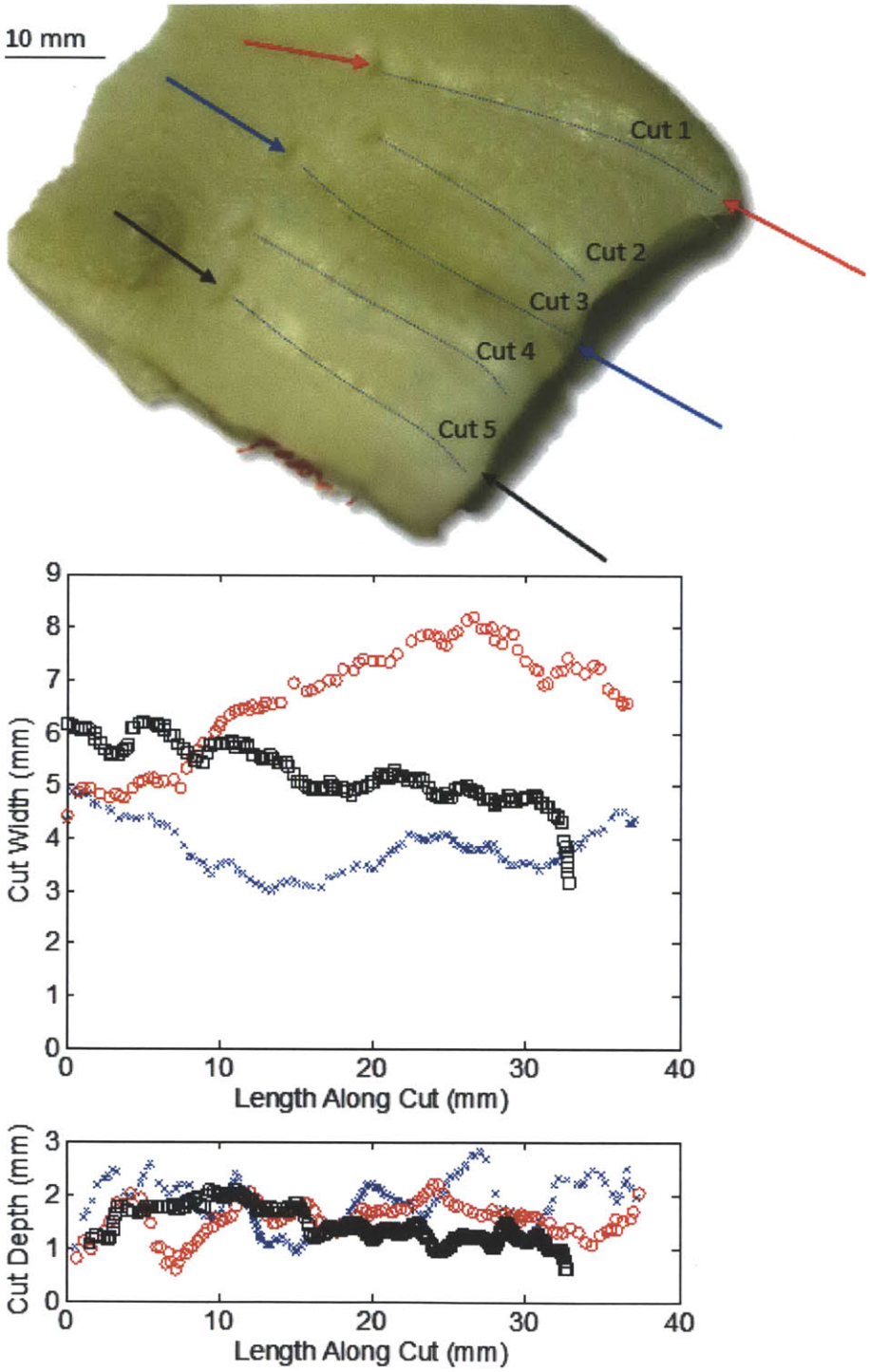

Figure 4-17: Cuts made in tissue treated with 10% acetic acid using 15 MPa and nozzles 4 mm apart intersecting at 120°. The colored arrows in the photograph show which cut is plotted in the graph showing cut dimensions, and blue dots trace each cut.

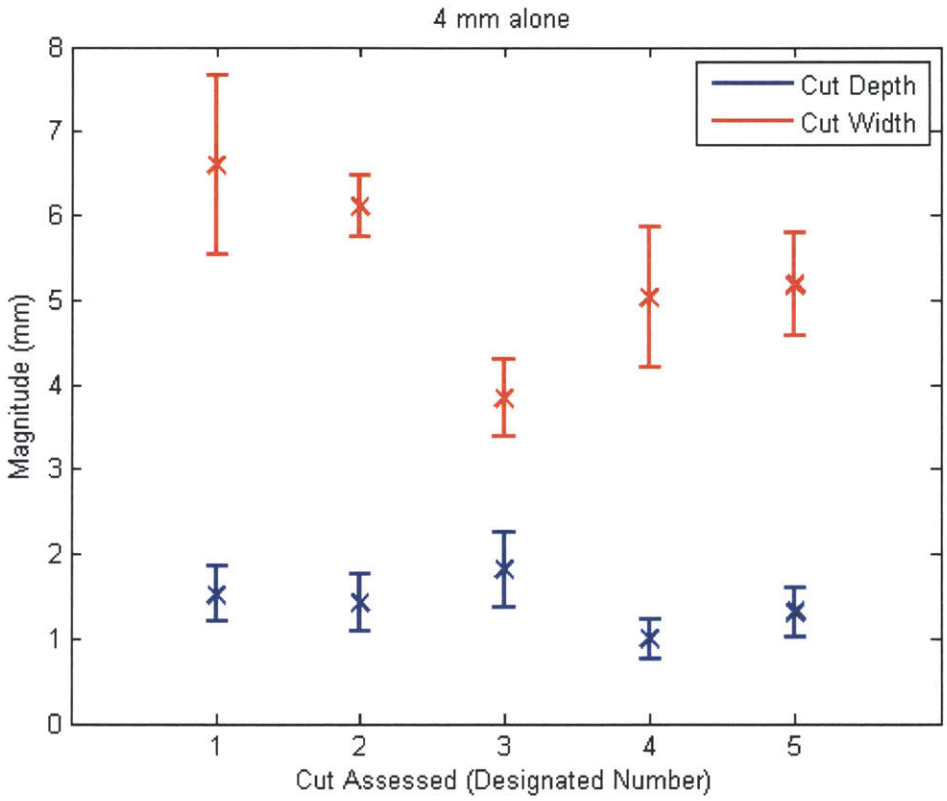

Figure 4-18: The average width and depth for the five cuts shown in Fig. 4-17. The bars indicate the standard deviation for each cut.

In Fig. 4-17, the depth of cut appears to vary with a higher frequency around a slowly changing average depth of cut. Contributing factors to these higher frequency variations include hand tremor, tissue variability, and imprecision in visually keeping the nozzle tips at the surface.

None of the five cuts shown was successful in completely excising the tissue. In each case, the jets failed to cut though either at the start or end of the pass, and in three cases there was at least one uncut strand of tissue midway along the pass. In order to take cut measurements, the separated piece was removed with thumb forceps.

This chapter showed that impinging jets are able to remove portions of necrotic tissue. The following chapter will detail additional tests and changes made to optimize the device performance.

Chapter 5

Optimizing Design for Cutting Necrotic Tissue

In the previous chapter, a dual-nozzle device with intersecting cutting jets was shown to be capable of excising discrete sections from eschar and sloughy wounds. To be considered a success in cutting sloughy wounds, however, many of the behaviors demonstrated in the eschar would need to be replicated: sections of the sample would need to be excised without damage to the adjacent tissue, and excised with enough control to remove a tissue layer via side-by-side cuts. In addition, a fully realized device would need to locally evacuate waste in order to prevent cross-contamination, and it would need to be demonstrated that the device did not propagate bacteria into the wound. Table 5.1 gives a summary of the configurations and methods that will be described in this chapter, and the effectiveness of each in accomplishing these goals.

Table 5.1: A summary of device performance with different cutting methods. A mark of '+' denotes satisfactory performance, a mark of '0' denotes inconsistent performance, a mark of '-' denotes an unmet criterion, and 'ND' denotes a criterion that was not determined. Except for the sample type labeled eschar, all tests were performed using simulated slough. The distance given in the description of each configuration refers to the distance between the cutting nozzles. Cuts made with the nozzles 4 mm apart had a jet intersection angle of 120°, and the tests performed at 2 mm apart had a jet intersection angle of 110°.

	Eschar, 2mm	4 mm	4 mm, vac	4 mm, vac, fast	2 mm	2 mm, pre-cut	2 mm, pre-cut, vac
No visible unwanted damage	+	+	0	0	+	+	0
Side-by-side cuts	+	-	-	-	-	-	+
Min cutting pressure (MPa)	15	15	15	15	10	7	6
Waste contained and evacuated	-	-	+	+	-	-	+
Bacteria not driven in	ND	ND	ND	ND	ND	+	+

5.1 Vacuum to Evacuate Tissue and Water

An attachment to apply suction at the cutting site was fabricated and tested on samples treated with acetic acid. The attachment, shown in Fig. 5-1, was made of Delrin [53]. The nozzle tips were covered by a central channel to which vacuum was applied through a 4 mm internal evacuation lumen. The sides of the channel were rounded in order to allow the attachment to glide over the tissue sample. A stainless steel plate hooked over the nozzle arms and served as an attachment point for the accessory. Tubing mated to a barbed fitting in the vacuum attachment, connecting the assembly to a suction canister. A GAST 053-V4F-G588DX vacuum pump applied suction to the canister [54], which collected water and detritus (Fig. 5-2).

Each cut excised and evacuated a section of tissue treated with 10% acetic acid, with water and debris locally contained. These cuts reliably excised tissue because, in addition to removing waste, the vacuum attachment gripped the tissue during cutting. The device was much easier to use with the vacuum attachment. Instead of visually guiding the nozzle tips at the surface, the user allowed the vacuum attachment to correctly position the nozzles. One disadvantage, however, was that because the nozzle tips were obscured, it was not possible to precisely guide the cut path. This visual obstruction meant that it was not possible to make side-by-side cuts.

Tests were performed both on samples that included the full dermis, fat, and muscle layers, and on samples with the fat and muscle removed. Any healthy live model would have all three layers. These isolated samples, however, lacked the lateral stiffness of their live counterparts. Removing the fat and dermis increased the lateral stiffness of the sample, compensating for this effect. Therefore, tests performed on samples with the three layers gave information about how the jets affected the deeper layers, while cuts made in dermis-only samples revealed behavior otherwise masked by the lateral flexibility.

Fig. 5-3 shows the measured dimensions for 11 cuts made with the vacuum attachment. In this configuration, the cuts made on multilayer and dermis-only samples

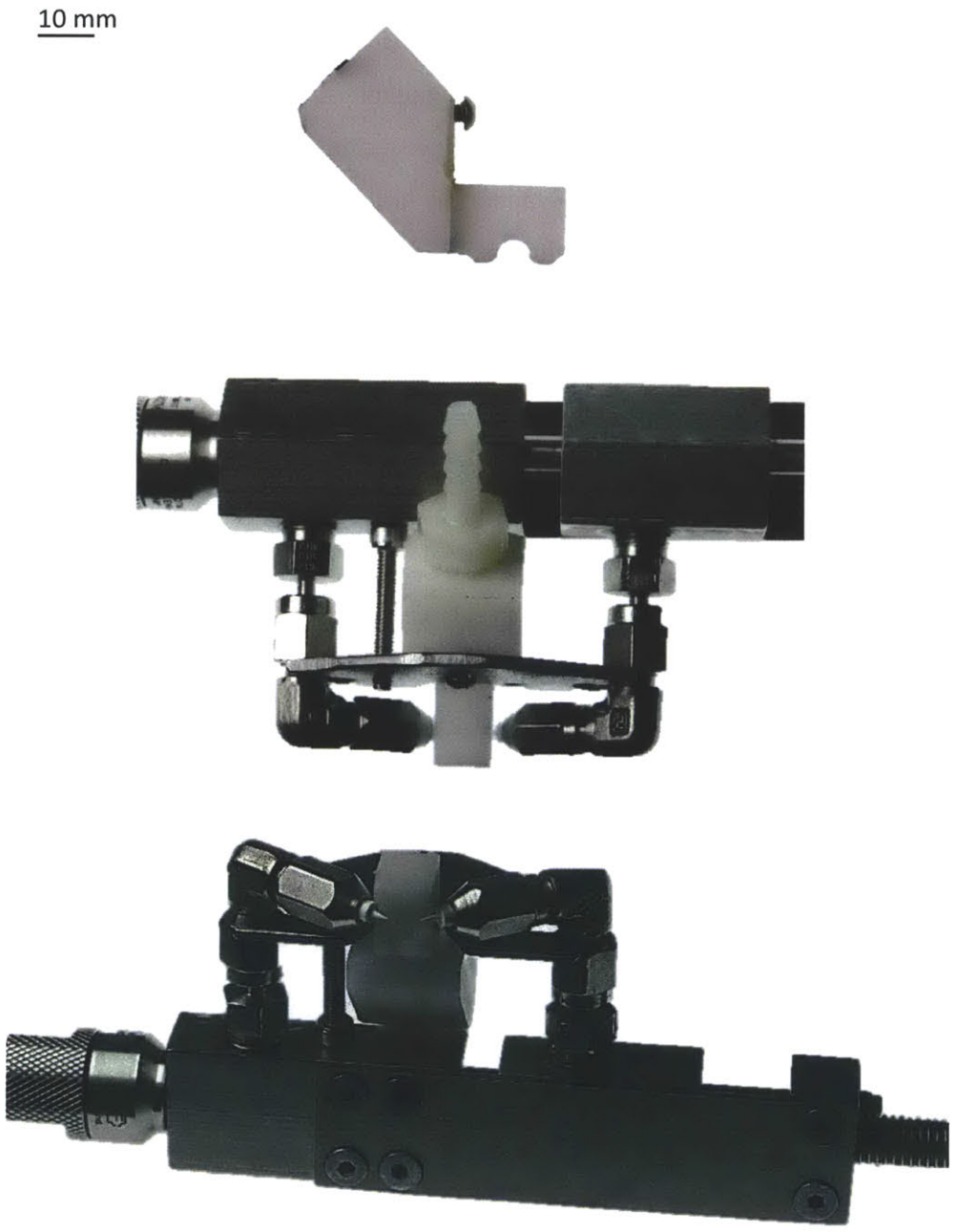

Figure 5-1: A vacuum attachment gripped the sample during cutting and evacuated water and excised tissue.

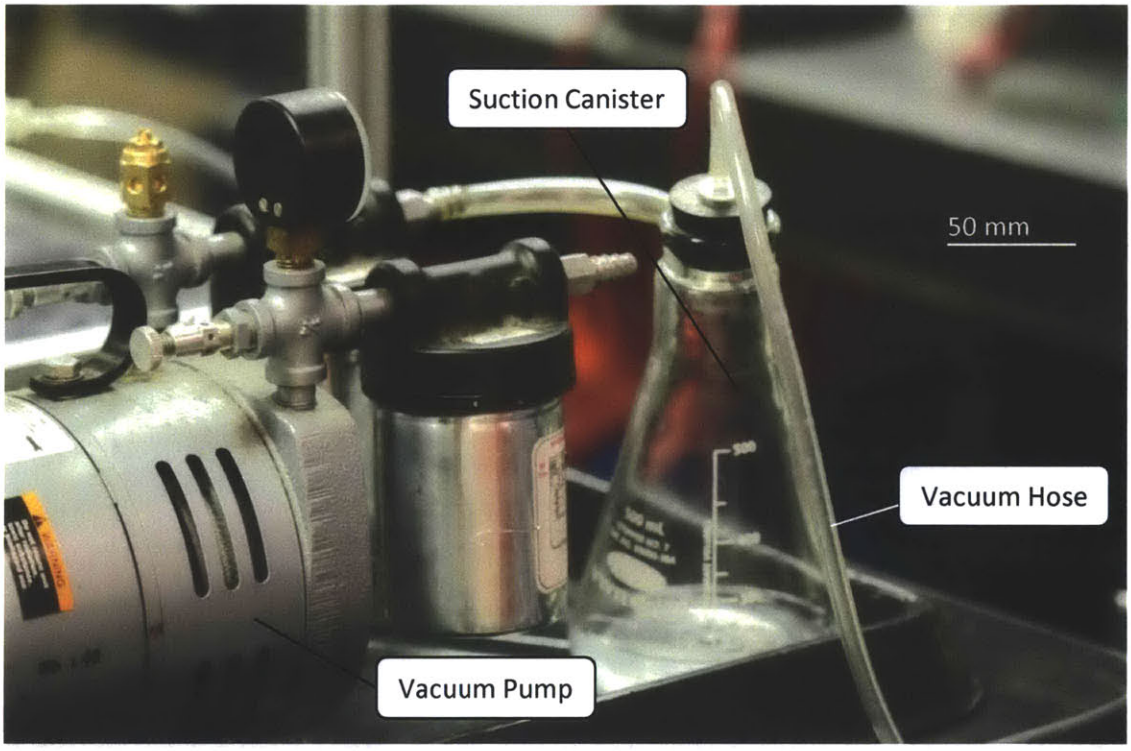

Figure 5-2: A vacuum pump applied suction to a canister that collected water and debris.

behaved comparably. Although the cuts made in the dermis-only samples are narrower and shallower, the difference in mean cut size is accounted for by a change in the positioning of the vacuum attachment between the cutting of the two samples; a similar jump in cut size is seen again in the final two cuts, after the attachment was again adjusted.

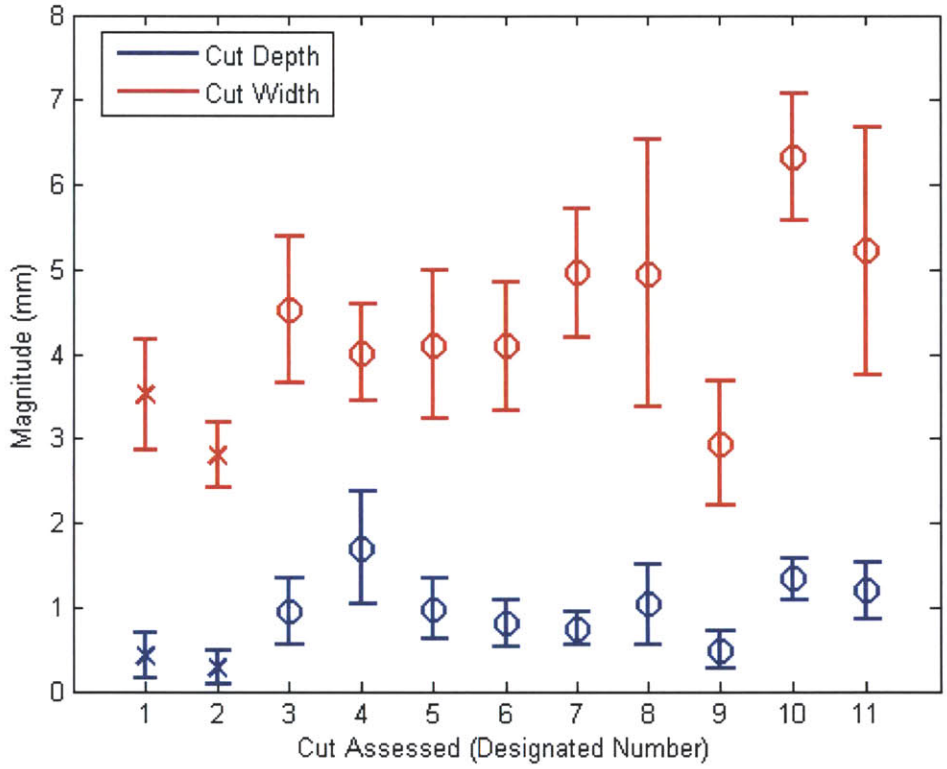

Figure 5-3: The average width and depth for eleven cuts made with a vacuum attachment. Cuts 1-2, 3-9, and 10-11 are made on the same sample. The 'x' indicates that the sample had the fat and muscle removed, while the 'o' indicates that the fat and muscle were intact. The bars indicate one standard deviation.

In spite of the increased ease-of-use provided by the vacuum, the standard deviation of the cut dimensions remains comparable to the behavior seen without the vacuum in Fig. 4-18. As before, the cut dimensions are affected by hand tremor and tissue variability, with the added factor that the angle at which the vacuum at-

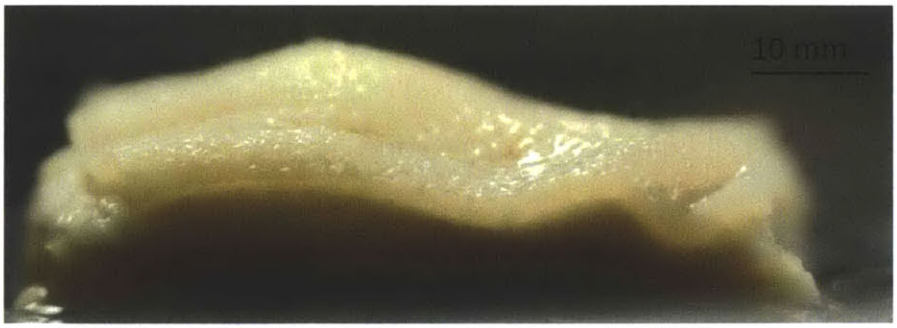

Figure 5-4: This sample bulges with injected water after a cut was made. Before the cut, the sample was flat and of a height equal to the current height of the right side of the sample.

tachment contacts the tissue changes how the tissue is held relative to the jets. The mean cut width and depth are likewise unchanged from the values measured without vacuum.

Water injection to the deeper layers was not noticeable during these cuts; the swelling was obscured by the attachment. Injection was shown to be present by weighing the sample before and after each cut, with the difference in weight due to injected water. The problem of water injection and ways to reduce it are discussed in the following section.

5.2 Reducing Water Injection

Cuts made in simulated sloughy wounds with the two-nozzle device would cause the tissue to visibly swell with water, as shown in Fig. 5-4. Excessive injection would cause injury to healthy tissue and thus is of concern.

In medicine, water injection injuries are usually seen in workers using high pressure fluids, such as pressure washers. Of primary importance in these injuries is treating any contaminants or bacteria that may have been injected with the water. The usual treatment for the water injection itself is to allow the body to resorb the fluid. In most cases full use of the injured body part is regained, though excessive water injection

itself can cause tissue necrosis [55]. The objective of debridement is to remove necrotic tissue, and so no debridement method should cause further necrosis.

Based on published limits for multiple needle injections to the same limb, $3\,L/m^2$ was defined as the maximum acceptable water injection level [56]. This injection limit is defined as injection permitted per surface area debrided. In the eleven cuts made with vacuum attachment, the water injection levels were highly variable, ranging from 1 to $29\,L/m^2$. Only one cut injected less than the $3\,L/m^2$ limit.

The following sections detail three efforts made to reduce water injection: translating the handpiece more quickly during the cut, moving the nozzles closer together and reducing the pressure, and initiating the cut with a scalpel blade running ahead of the nozzles in order to further decrease the required cutting pressure. For each method, there is sizable spread in injection levels, as shown in Fig. 5-5. Moving faster was successful in reducing water injection, but with a tradeoff in cut quality. Reducing the nozzle distance caused no change in injection per area debrided. The pre-cutting with blades was effective for thin samples, but using blades with samples that had fat and muscle intact caused an increase in water injection, particularly when a vacuum was applied as well. In cuts made on thin samples with blade pre-cutting and vacuum, water injection for three out of five samples was $7\,L/m^2$ or less. The other two samples had a higher level of injection, showing the effect of tissue variability. Thus, further reduction in water injection is required, as is more consistency across samples.

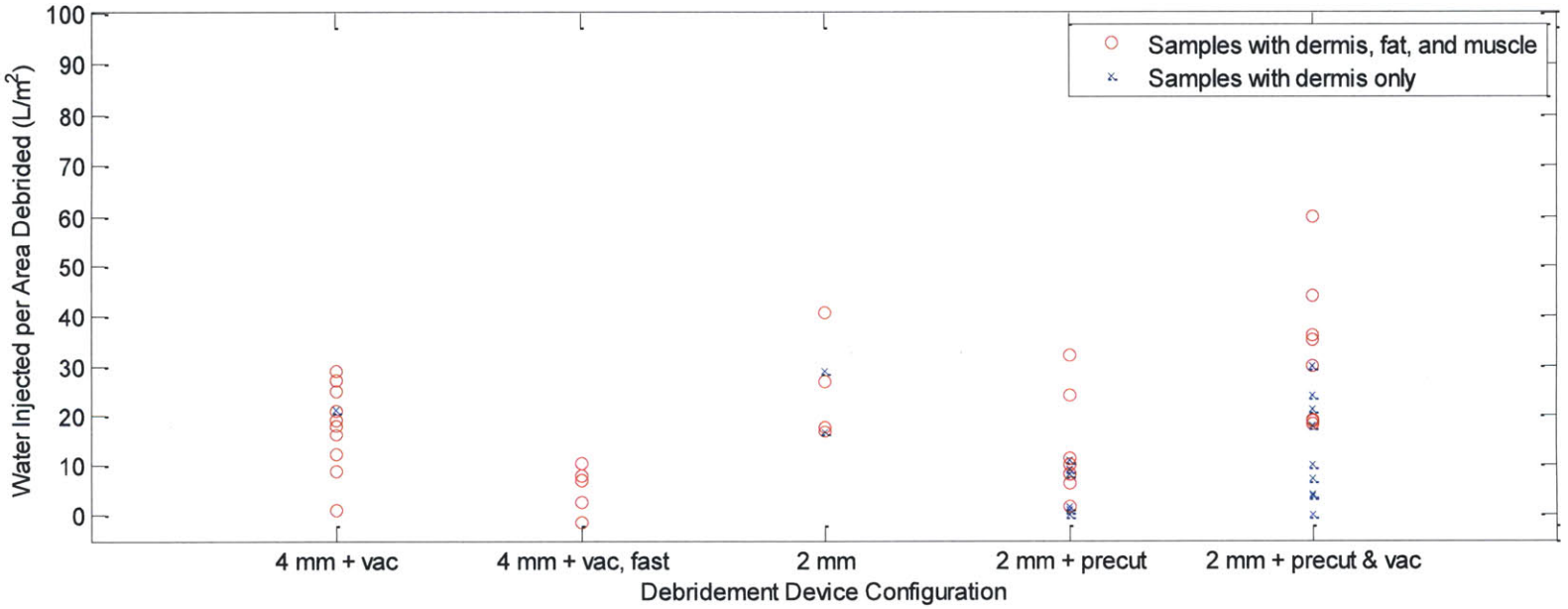

Figure 5-5: The levels of water injection measured for each method of cutting. Each data point corresponds to the injection level measured for a single cut.

5.2.1 Increasing Speed of Cut

The first measure taken to reduce water injection was to test the effect of translating the handpiece more quickly during the cut. With the jets spending less time in contact with the tissue, the water injection over the entire cut should be reduced. The handpiece during these tests translated at a rate of about 15 mm/s, while in previous tests the rate of travel was about 4 mm/s. The nozzles were positioned 4 mm apart, intersected at 120°, and the vacuum attachment was employed.

These faster passes were successful in reducing the volume of water injected to a range spanning between 0 (no water injected) and $10\,L/m^2$ for five measured cuts. However, cutting was inconsistent, with failure to cut often occurring at the beginning and end of the cut. Because of the speed of translation, the jets were not optimally positioned relative to the tissue at every point in the cut, which resulted in the cutting inconsistencies. When the excised portion remained attached at any point, no tissue was evacuated.

Should future improvements optimally position the nozzles relative to the tissue throughout the cut, these faster passes would become a viable operating technique. For the most part, dermal whitening was not observed, meaning that water was not injected into the skin surface. Fig. 5-6 shows a cut with whitening only at the start, the location where the jets did not cut through.

Because the vacuum had less time to draw tissue up between the cutting jets, these faster cuts showed a decrease in cut dimensions. The average depth for the faster cuts ranged from 0.2 to 0.8 mm, compared to a depth of 1.2 and 1.3 mm measured for slow cuts made on the same sample. Likewise, the depth decreased from 5.2 and 6.3 mm on average for the slow cuts to 3.3 to 4.4 mm on average for the fast cuts. There was no change observed in the standard deviations for the fast and slow cuts. Fig. 5-7 summarizes the dimensions measured for five fast cuts.

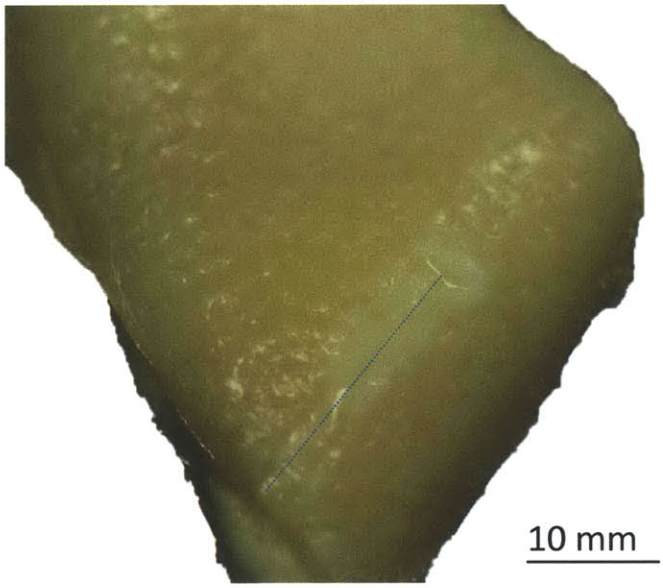

Figure 5-6: Little whitening was produced on the fast cuts made with a vacuum employed. The path of one such cut above is traced by the blue dotted line.

5.2.2 Shortening Nozzle Distance

Lowering the flow rate of the cutting jets by decreasing their pressure was hypothesized to reduce water injection. By reducing the distance between the nozzle tips from 4 mm to 2 mm, the jets cut through less material before impinging. Less cutting energy was required, and the necessary pressure was reduced from 15 to 10 MPa. The nozzle angles at this shorter distance also decreased from 120° to 110°. Unfortunately, these changes did not result in reduced water injection: in two cuts made on thin acid-treated samples, the water injection measured 17 and 20 $\mathrm{L/m^2}$, exactly in the range observed for cuts made at 15 MPa. Although less water was injected per length of cut, a narrower area was debrided with the nozzles closer, resulting in no net change in water injection.

The water injection is shown visually in Fig. 5-8. This cut, made with 0.25% bromophenol blue dye solution, shows that injected water spreads radially outward from the tip of the cutting V and is particularly concentrated in line with the two cutting jets.

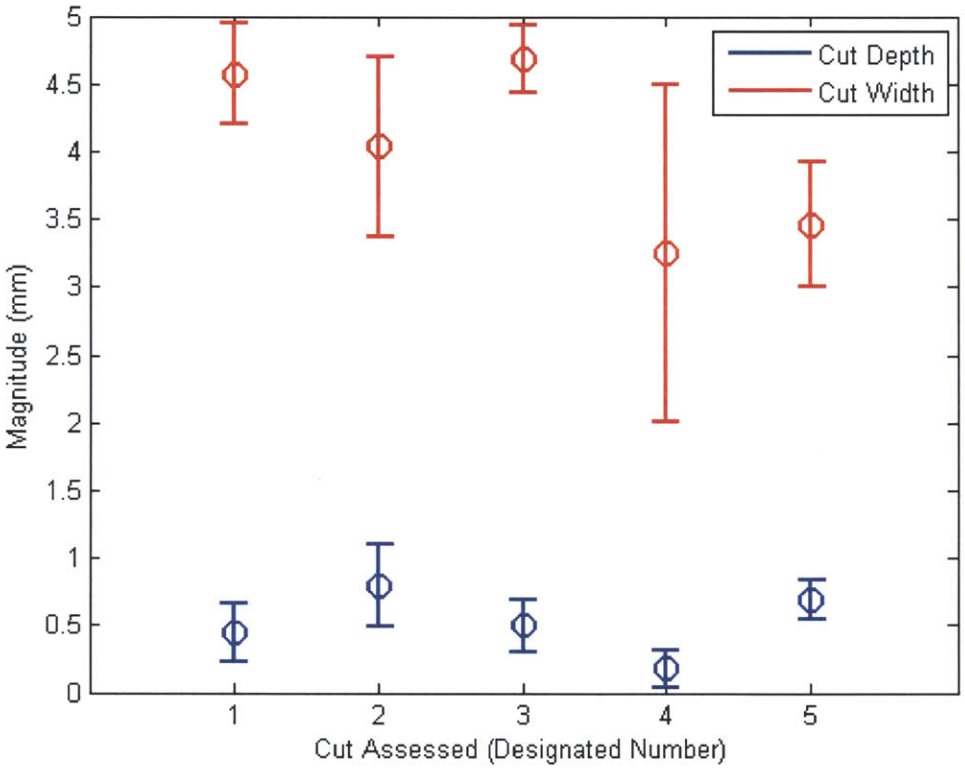

Figure 5-7: The average width and depth for five cuts made while applying vacuum at an increased translation speed of 15 mm/s. The 'o' indicates that the fat and muscle were intact on the sample. The bars mark one standard deviation.

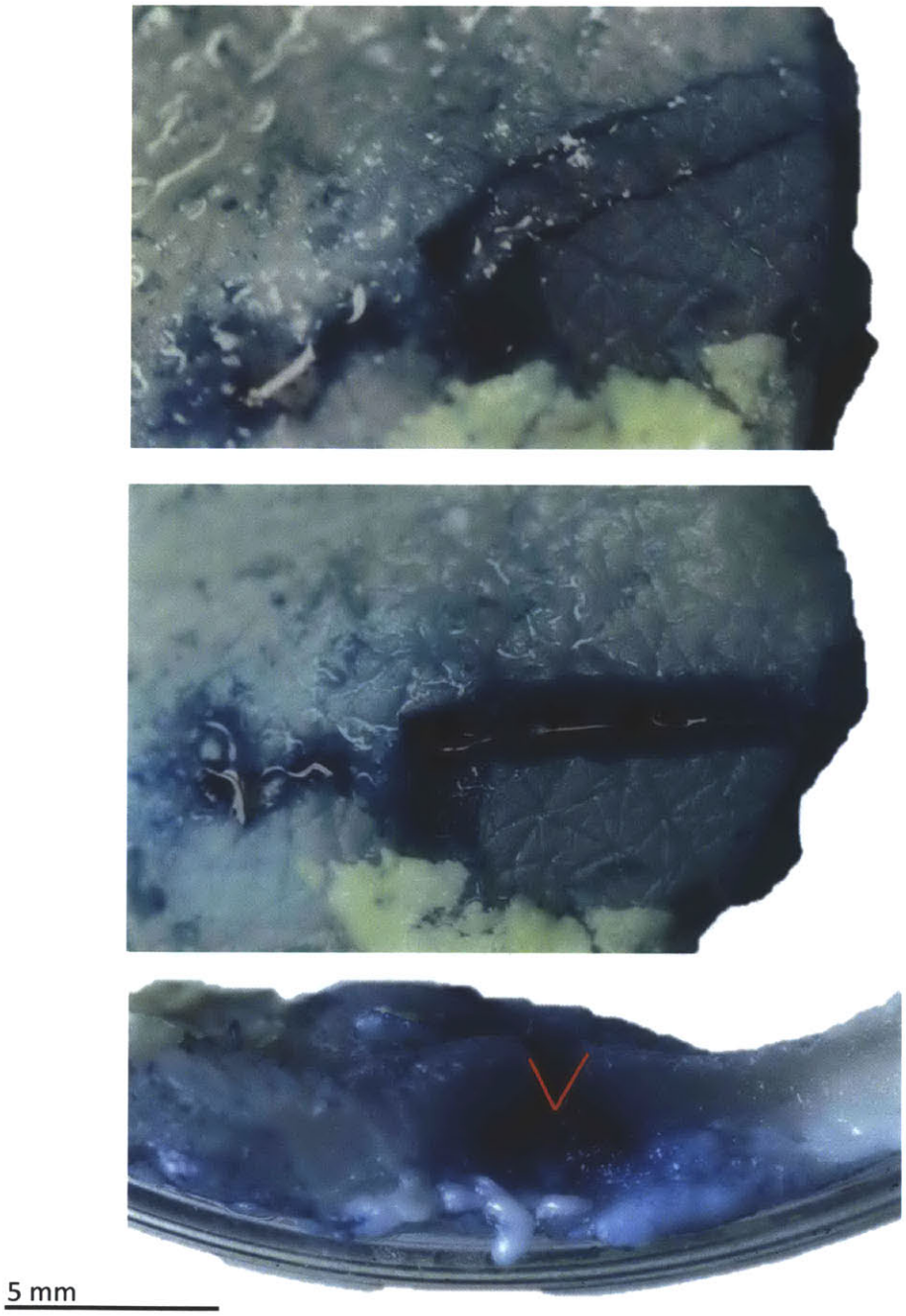

Figure 5-8: A cut made with 0.25% bromophenol shows how injected water is distributed in the sample. The top picture has the excised portion in place, the middle picture shows that portion removed, and the bottom image is a cross-section of the cut, with the section excised by the cutting V outlined in red.

When cutting with 10 MPa in a dermis-only sample, whitening showed that water was injected into the surface only the start, which was the only uncut portion. This sample nevertheless absorbed all the injected water into its single layer; only when a second cut was made at 15 MPa did water exit through the base of the sample. Fig. 5-9 shows both cuts, and Fig. 5-10 shows the dimensions of the cut made at 10 MPa alongside a representative earlier cut.

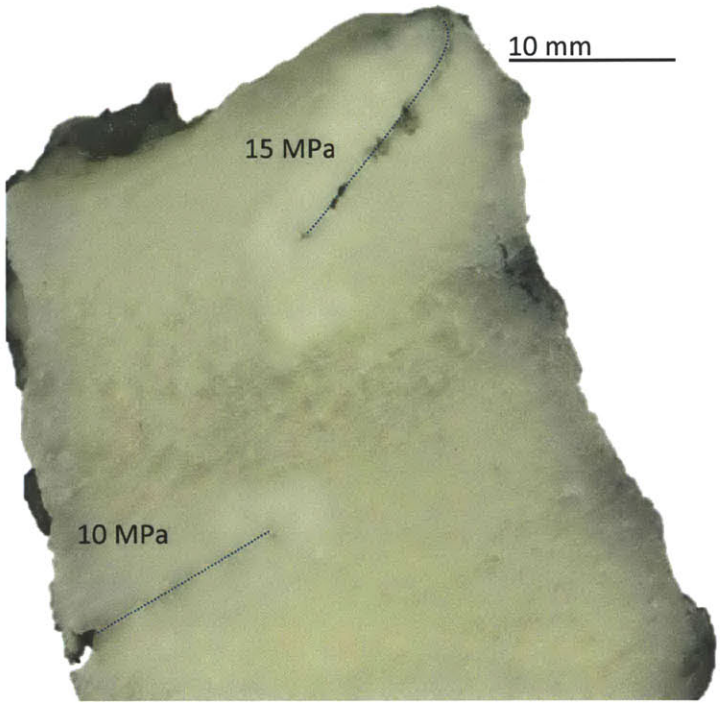

Figure 5-9: With the nozzle tips spaced 2 mm apart, cutting at 15 MPa causes the sample to turn white, but 10 MPa produces whitening only at the cut start. Blue dotted line traces cut path.

Cuts made in multilayer samples behaved less ideally. Without vacuum gripping the cutting area, the sample would move laterally relative to the nozzle tips, causing water to inject into the surface for each of the seven cuts made, with the characteristic whitening shown in Fig. 5-11. The sample instability also resulted in shallower and narrower cuts.

Even though water injection was not affected, shortening the nozzle distance was a

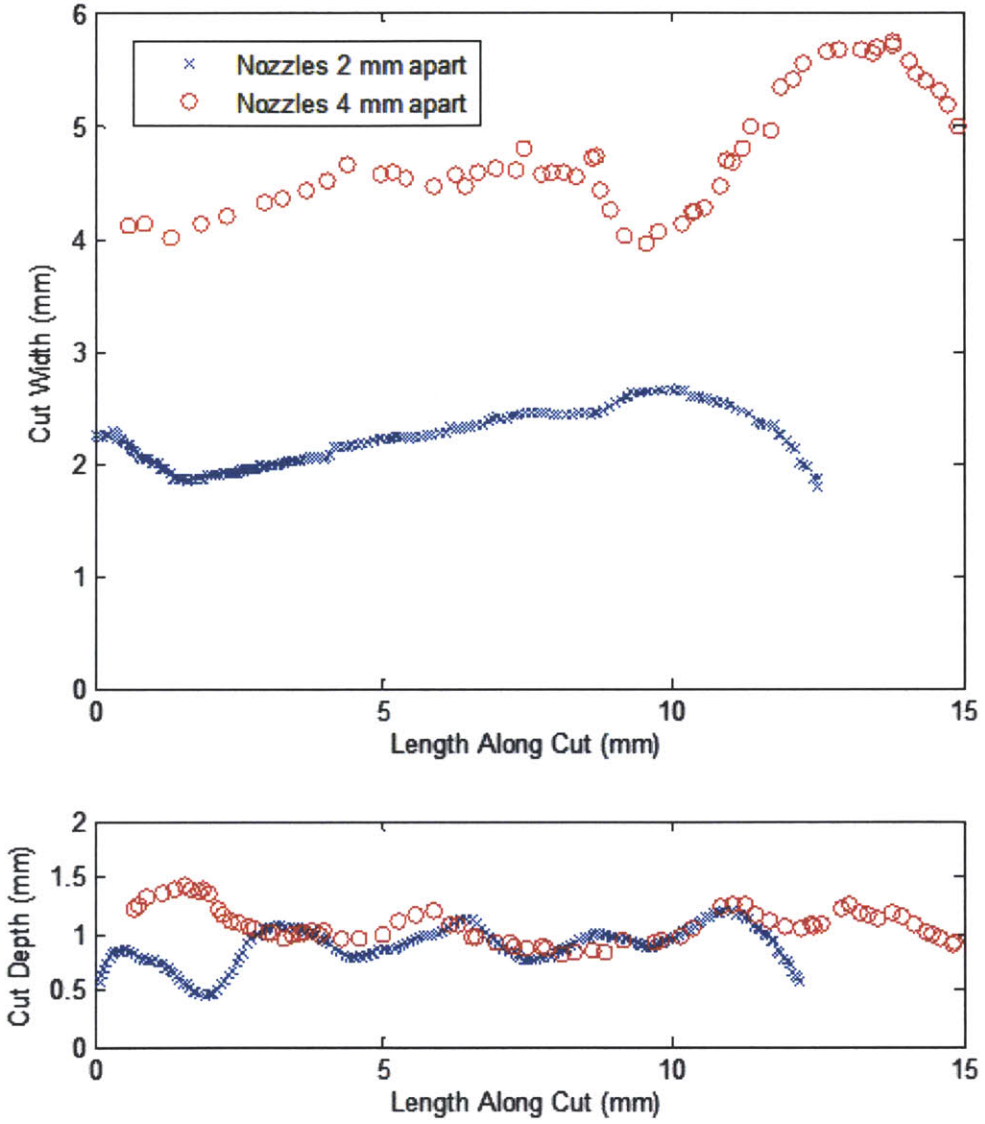

Figure 5-10: The cuts are narrower when the nozzles are closer. The average width is close to the nozzle tip distance: 2.2 mm, with a relatively low standard deviation of 0.2 mm. The expected depth based on the dimensions of the cutting triangle is 0.7 mm. The measured average depth is slightly higher at 0.9 mm, with a standard deviation of 0.2 mm.

Figure 5-11: Cuts made on a sample with fat and muscle produced whitening. These cuts were shallower and narrower than cuts made in dermis-only samples: one measured an average depth of 0.4 mm with a standard deviation of 0.2 mm, and an average width of 1.8 mm with a standard deviation of 0.4 mm.

favorable change, because the reduced pressure placed a lower demand on the pump, and the narrower cuts allowed finer control over the areas debrided.

5.2.3 Pre-cutting with a Surgical Blade

More energy is required to start a cut in tissue than to propagate one [25]. It was hypothesized that by initiating a cut by scoring with a scalpel blade, less pressure would be required to complete the cut. With the lower flow rate and less cutting energy, reduced water injection was expected. In preliminary testing, a scalpel blade run lightly over the surface of acid-treated tissue created an incision 0.5 mm deep. This initial cut was followed by a single nozzle directed into the small incision. With 5 MPa cutting pressure, the initial incision deepened to 3 mm. When the same jet was directed at tissue with no pre-cut, water was injected, but no incision was effected.

Based on this initial success in reducing cutting pressure, small blades were selected to run in front of each cutting jet in the two-nozzle device. These blades, comparable to X-ACTO X3241, had a 3.5 mm long cutting length and are shown in Fig. 5-12. Delrin attachments mounted the blades to the nozzle arms. These attachments have a slightly undersized 11 mm hole; four cuts along the walls of this hole gave it the flexibility to slide onto and grip the threaded nozzle caps, also shown in Fig. 5-12. The Delrin attachments have a pocket to hold the blades and position them adjacent to the nozzle tips. The blades are secured with an M2 set screw.

Fig. 5-13 illustrates the process of pre-cutting with the blades. The Delrin attachments secure the blades immediately in front of the nozzles. During debridement, the blades score the tissue, and the fluid jets deepen the cut. The cut shown in Fig. 5-14 was made in acid-treated tissue using this method. The nozzle tips were 2 mm apart, angled at 110^{circ}, and a cutting pressure of only 7 MPa was needed, compared to the 10 MPa needed to cut without the blades.

The water injection was significantly reduced, ranging from 0 to 11 L/m^2 in thirteen cuts made with pre-cutting, compared to the 17 and 20 L/m^2 measured in two

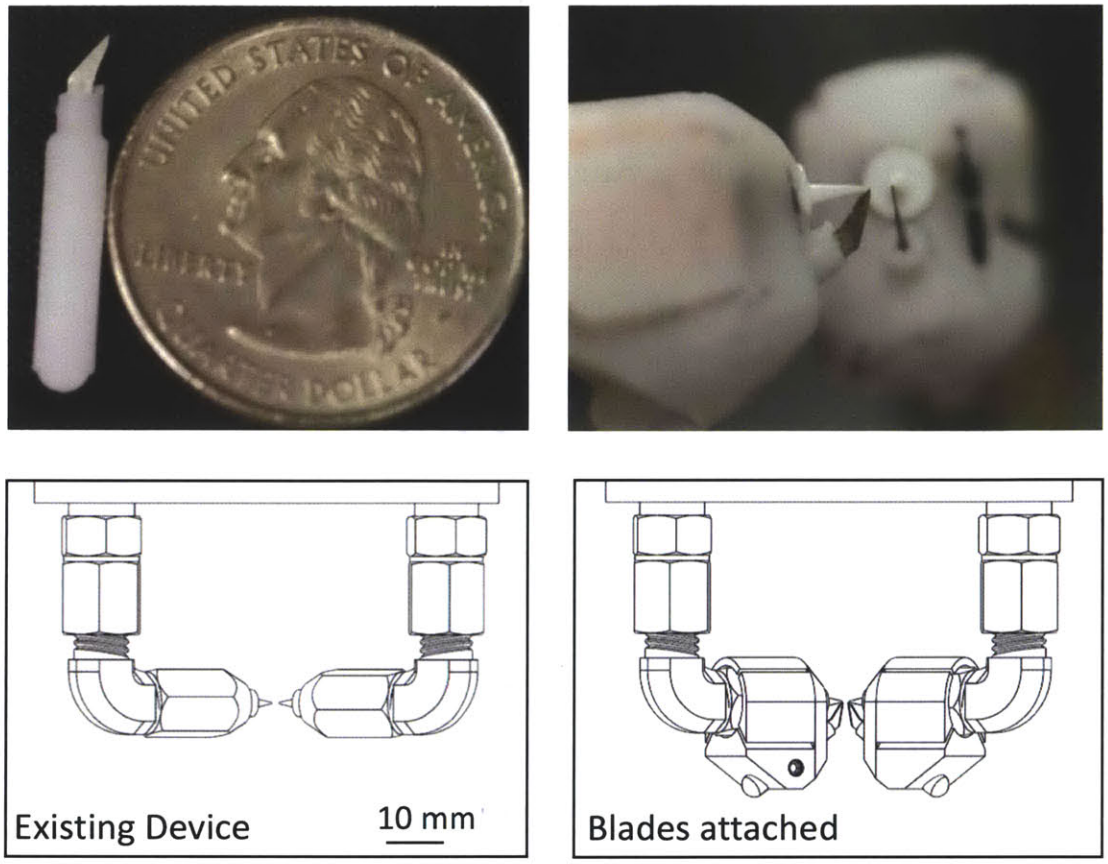

Figure 5-12: Small blades were mounted in front of the nozzles using Delrin attachments that snapped onto the nozzle arms.

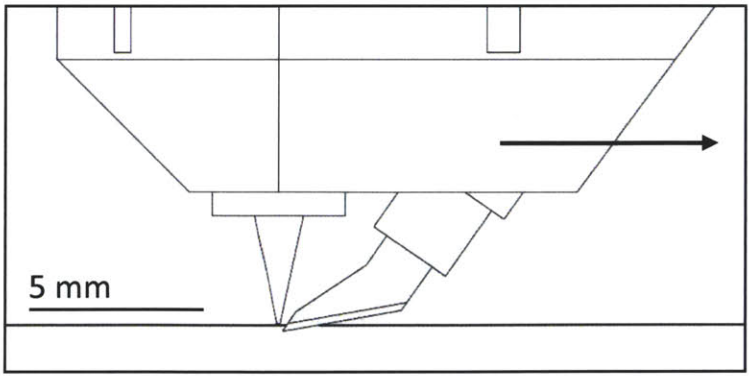

Figure 5-13: The surgical blade initiates an incision. The cutting jet follows behind and deepens the incision. Less pressure is required to cut when the incision is started by the blade.

Figure 5-14: Cut made with blade pre-cut. Blue dotted line traces the cut path.

cuts without pre-cutting. This reduced injection range matches the one measured for the fast cuts discussed in Section 5.2.1, and as with those cuts, the injected volume with pre-cutting was rate dependent. Cuts routinely progressed at 4 mm/s. A cut made in a multilayer sample at a reduced speed of about 1 mm/s injected water at an inflated rate of $32\,\mathrm{L/m^2}$.

Because the blades were mounted parallel to the nozzles, they contacted the tissue at a relatively shallow angle. Downward pressure was applied to ensure that both blades made cuts. Whether a portion was excised depended on how successfully the blades made incisions in the tissue. Applying the requisite force was achievable in both sample types, though in the multilayer samples careful manual restraint of the sample surface was necessary. The engagement of the blades anchored the sample surface relative to the jets, resulting in equivalent cutting performance in the multilayer and dermis-only samples. Five out of seven passes made in dermis-only samples and four out of seven passes in the multilayer sample were cut along the entire length; the uncut sections occurring where the blades were not engaged.

Increasing the downward force on the handpiece caused the blades to sink more deeply into the tissue. Because the blades were angled outwards, this measure increased the width of cut, which in some cases expanded to over 3 mm. Fig. 5-15 gives the dimensions of four cuts. In addition to their equivalency in the volume of

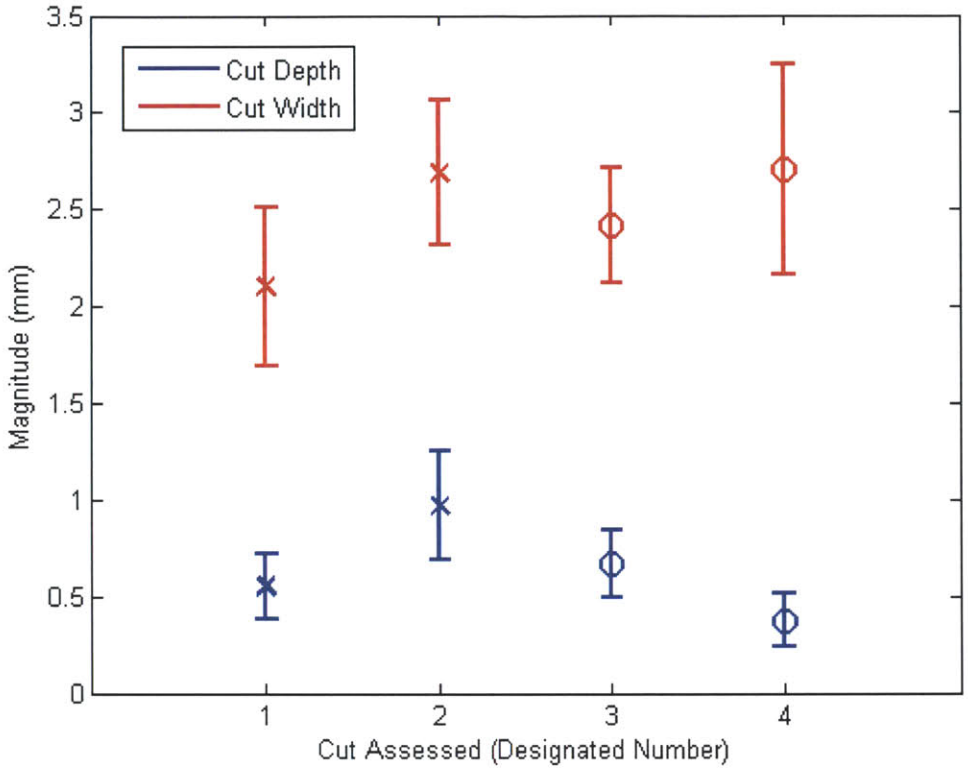

Figure 5-15: The average width and depth for four cuts made with the blades pre-cutting. The 'x' indicates that the sample had the fat and muscle removed, while the 'o' indicates that the fat and muscle were intact. The bars mark one standard deviation.

water injected and tissue excision, cuts made in multilayer and dermis-only samples were also comparable in dimension.

Integrating Vacuum and Blades A vacuum attachment was made to fit around the blades, as shown in Fig. 5-16. The evacuation lumen was 3 mm in diameter. This vacuum piece mounted to the same steel plate as the previous vacuum attachment, and as before this piece connected to the vacuum supply via a barbed tube fitting. Unlike the prior attachment, this one was narrow enough to allow visual guidance of the cut path. Two pictures of the device and a diagram of the internal flow structure

are shown in Fig. 5-16.

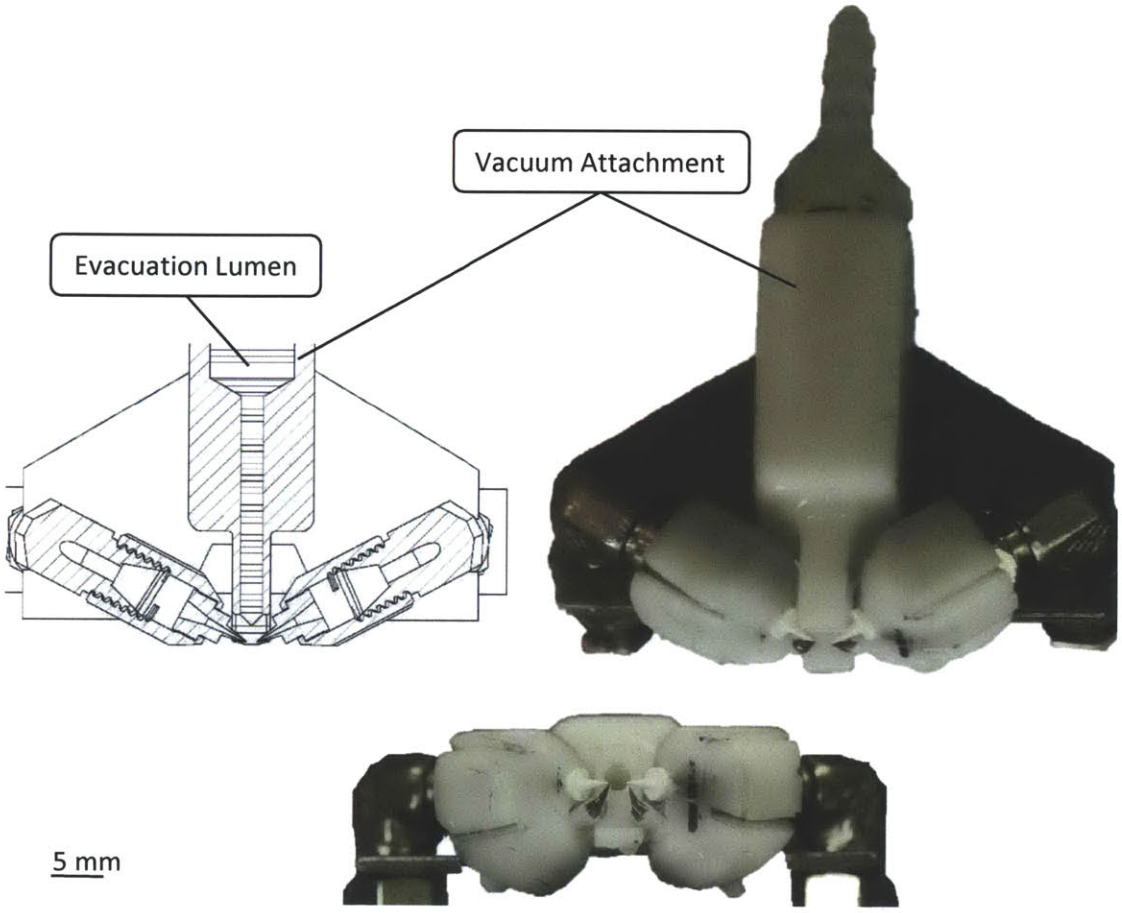

Figure 5-16: A vacuum attachment was made to fit over the blades.

When cutting with the blades with the vacuum attachment, the equivalent behavior in the multilayer and dermis-only samples vanished. With the vacuum attachment in place, less downward force could be applied to the flexible multilayered samples, preventing the blades from cutting deeply enough to hold the surface relative the the jets. The same five samples were each tested twice, the first time with fat and muscle intact, and then again with only the dermis. While in the multilayer state, water injection ranged from 18 to 92 L/m^2 measured over nine cuts. With only the dermis, this injection range decreased to 0 through 24 L/m^2 measured over eleven cuts. Fig.

5-17 illustrated that with the layers intact, the edges of the cuts would pucker and whiten, but cutting only the dermis of the same sample would leave a smooth edge and discolor only with the subsurface injection visible through the translucent top layer. Surface whitening was visible in four out of the five multilayer samples, but in only two of the five dermis-only samples.

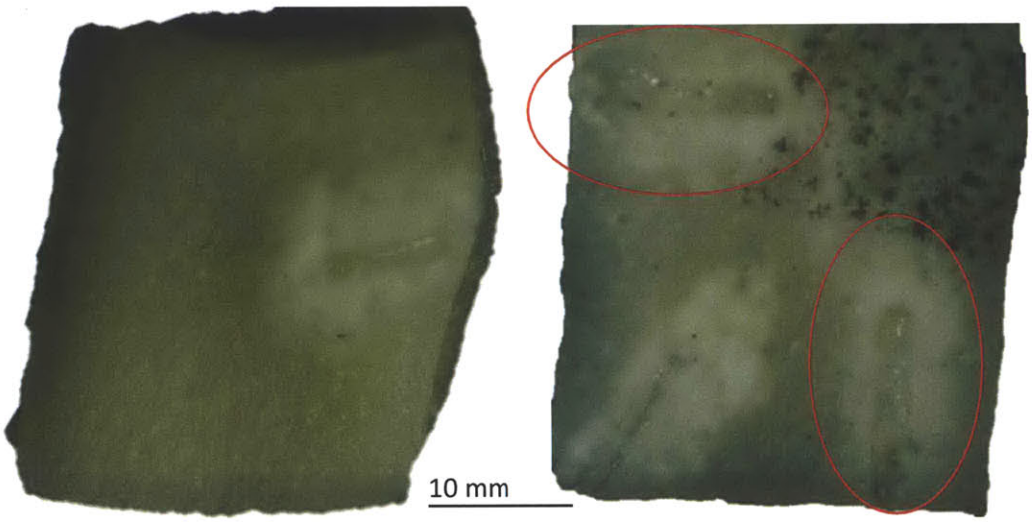

Figure 5-17: Post-mortem porcine abdominal tissue. On the left the sample with fat and muscle intact, on the right the same sample with fat and muscle removed. The cut in the left picture shows more whitening and puckering than the two cuts circled in the right picture, which were made after the fat and muscle were removed. The top right corner of the sample was speckled with spray paint in order to increase the fidelity of a 3D image rendering of the cut. Nozzle tips were 2 mm apart, jets intersected at 110°, and pressures of 6 or 7 MPa were applied.

Tissue variability between samples was prominent in these series of tests, with samples showing the same trends whether multilayered or dermis-only. At the upper end of the water injection range was a single sample that, when cut at equivalent conditions, absorbed twice as much water as the average rate across the five samples. Another sample required a higher pressure to excise tissue. Where sections were excised from the other samples at 6 MPa, this one required 8 MPa. If these two samples are excluded when considering the dermis-only testing, the water injection for the remaining seven cuts ranged from 0 to 10 L/m^2, equivalent to the water injection

measured for pre-cutting without vacuum.

One factor that negatively impacted the consistency of performance across samples was the shallow angle at which the blades entered the tissue. For the blades to make an incision, a force was pressing their edge into the sample was required. Because the two blades installed parallel to the nozzles were directed in opposite directions, any sideways force on the handpiece would cause one blade to make a deeper incision than the other. Downward force was required to make incisions with both blades simultaneously. If the blades were at an angle closer to normal to the surface, then less downward force would be required to initiate both incisions, and because of this decreased required force, the blades would cut more reliably, potentially increasing the performance consistency between samples. With the blades cutting more reliably, water injection would likely also be reduced, both because it was observed that less water was injected when the blades made deeper incisions, and also because it would be possible to translate the handpiece more quickly.

Further improvements in the volume of water injection would be possible if the sample surface were under tension. Less force is required to make incisions in tissue experiencing tension [57], and it was noted in previous tests using a single nozzle that any tension applied to the sample increased the depth of cut. By creating an attachment that tensioned the sample subject to the blades and cutting jets, the pressure required to excise tissue would be firth reduced, which could potentially lead to a decrease in volume of injected water.

Regardless of variations in sample layers or the volume of water injected, the device excised a strip every cut. As with the previous vacuum attachment, applying suction removed the need to precisely position the nozzles at the sample surface. In some cases, when the lip of the vacuum channel reached the sample edge, the device would lose suction and the end of the strip would not cut through. When the strip was completely excised, it was successfully evacuated through the suction lumen.

The suction drew the sample upwards into the vacuum channel for both the multi-

layered and dermis-only samples, increasing the width of cut relative to those without vacuum. Dimensions for selected samples are given in Fig. 5-18.

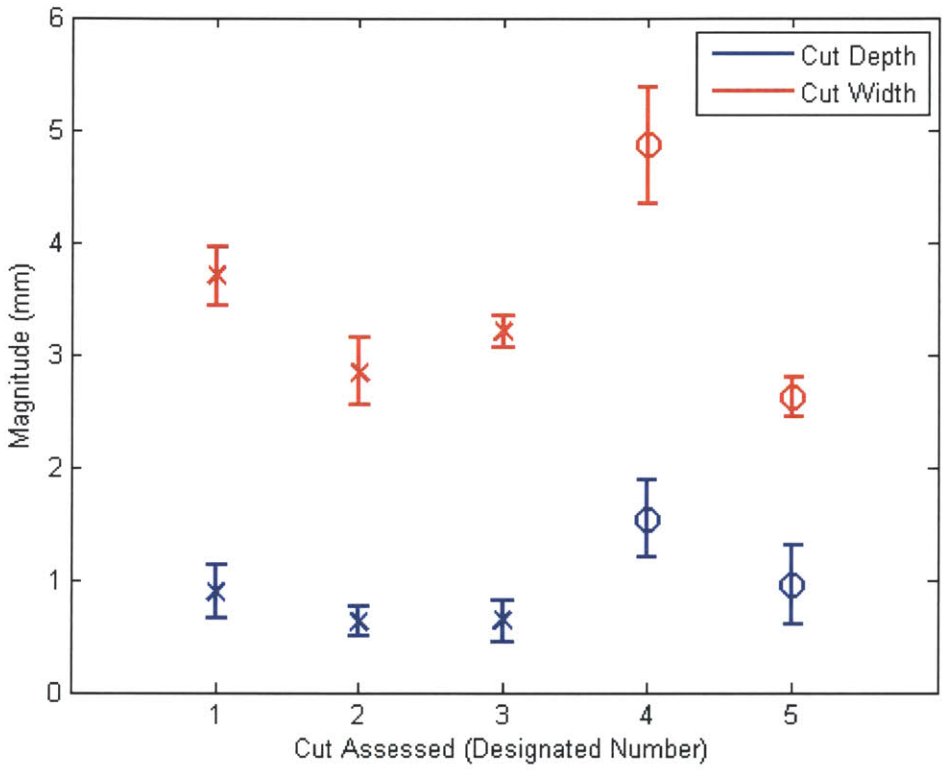

Figure 5-18: The average width and depth for five cuts made with vacuum and blades pre-cutting. The 'x' indicates that the sample had the fat and muscle removed, while the 'o' indicates that the fat and muscle were intact. The bars mark one standard deviation.

With this narrow vacuum attachment, the tissue was excised so reliably that clearing a section of the sample using side-by-side cuts became possible, a capability previously demonstrated only in cutting acrylamide and eschar. Fig. 5-19 shows a 15 mm by 20 mm area debrided by six parallel cuts. The remaining surface shows a rise and fall made by the cutting V, similar to the texture seen in cutting acrylamide. These cuts were performed on a multilayered sample.

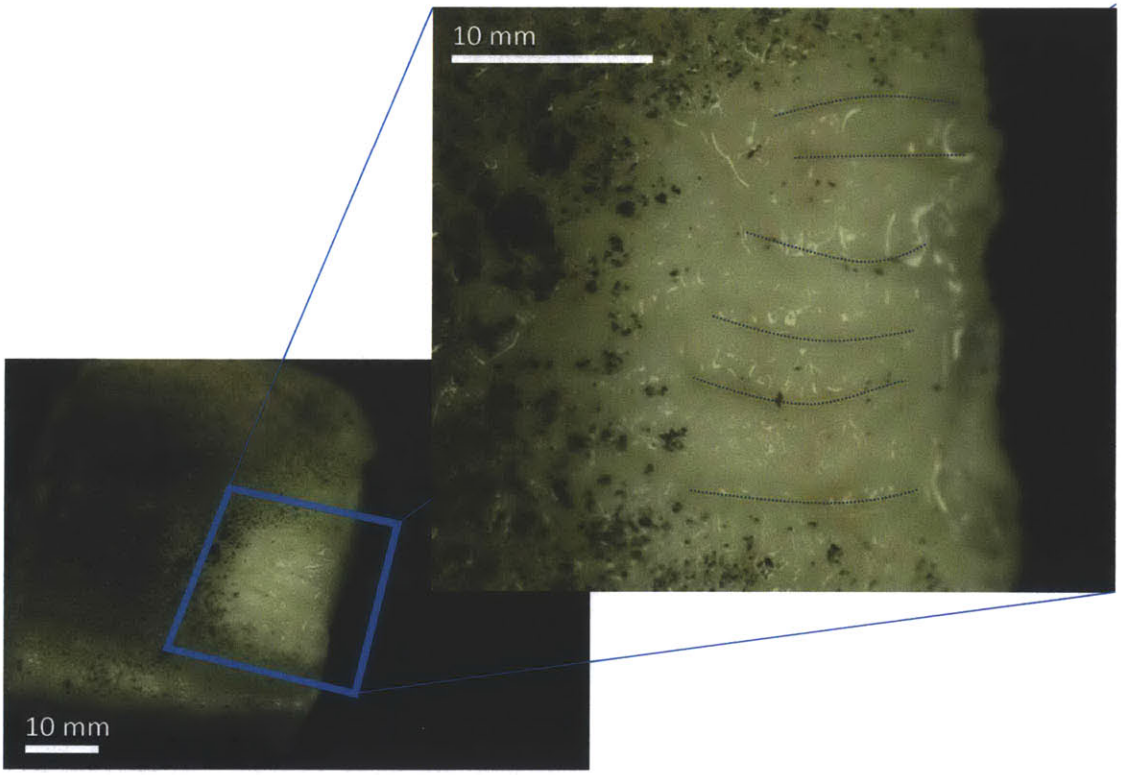

Figure 5-19: It was possible to make side by side cuts with blades and vacuum, as shown by the six adjacent cuts above.

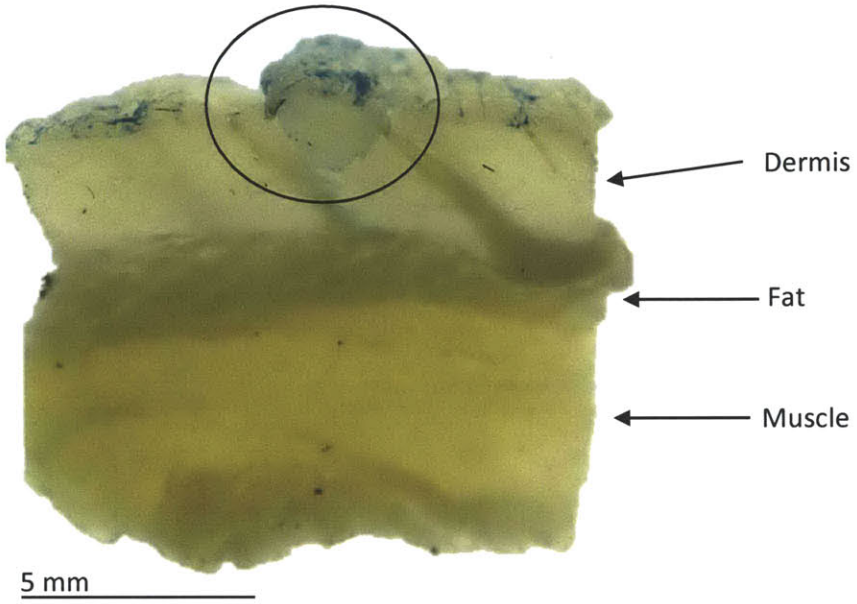

Figure 5-20: A cross-section of a cut made in a sample seeded with 1 µm blue polystyrene beads. The excised strip is still in situ. No blue beads have visibly been driven into the sample.

5.3 Assessing if Bacteria are Driven into Tissue

As discussed in Section 2.2.1, high pressure lavage has been shown to propagate bacteria deeper into soft tissue. Because the dual nozzle device directs high pressure jets into the tissue, this was a concern. To assess whether the device would propagate bacteria into tissue, a 35 mm by 35 mm acid-treated sample was seeded with 0.1 mL of a solution that contained 1 µm blue-dyed polystyrene microspheres at a concentration of 4.55×10^{13} particles/L [58]. A cut was made in this sample with the nozzle tips spaced 2 mm apart, an intersection angle of 110°, and blades installed for pre-cutting. A cross section of the resulting cut is shown in Fig. 5-20. Because a vacuum was not used for this particular experiment, the excised strip is still in situ. A small amount of blue is visible along the edge of this strip, though all the blue does appear to be contained on the strip. No blue has visibly been driven into the underlying tissue.

The test was repeated with a doubled volume, 0.2 mL seeded onto a sample of

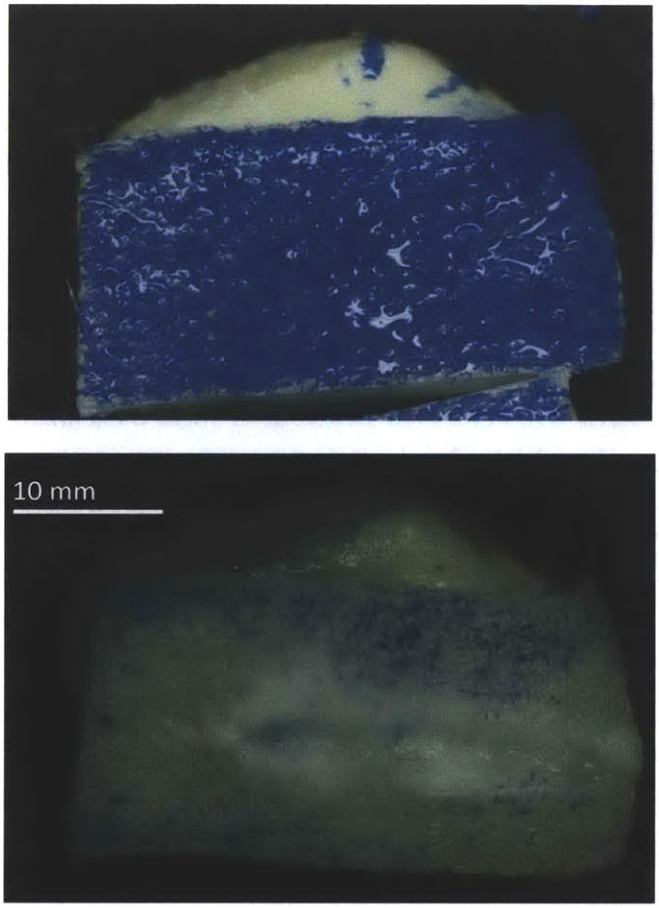

Figure 5-21: Before and after cutting with blades and a vacuum employed. Parameters for cutting were a pressure 6 MPa and a 110° intersection angle with nozzles 2 mm apart. The tissue surface was seeded with 1 µm blue-dyed spheres.

the same dimensions, 35 mm by 35 mm. This time, a cut was made using blades and vacuum. An image of the sample before and after the cut is shown in Fig. 5-21. Most of the beads were washed away by the lavage of the mist from the intersecting jets, though care was taken to direct the mist away from the as-yet uncut area, meaning that each area was exposed to the cutting fluid only as the jets passed by.

Parts of the resulting cut show a slight blue tinge, indicating the presence of the microspheres. These spheres are likely present due to water containing the beads running into the trough after the cut was made, a problem which could be solved by

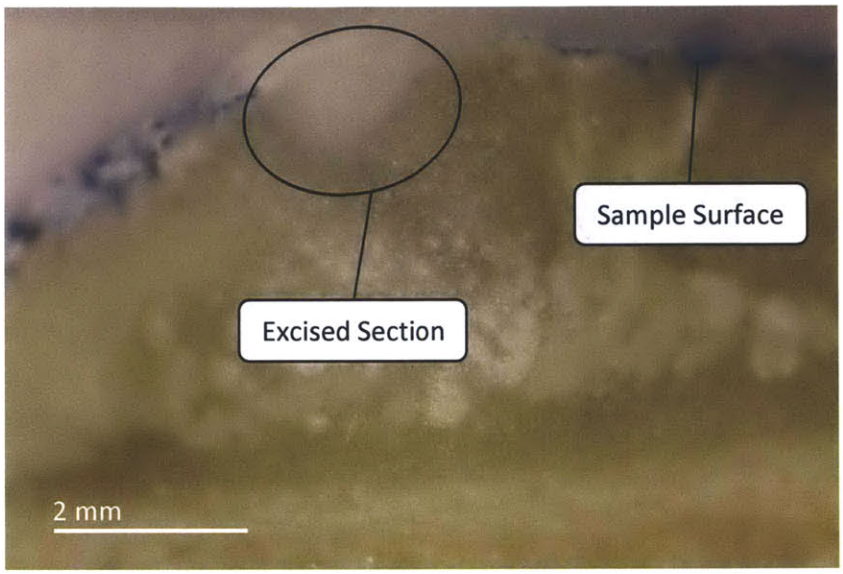

Figure 5-22: A cross-section of a microbead-seeded sample in a cryotome. The blue on either side of the excised section shows the presence of the beads on the untreated surface. No blue beads are visible in the excised section.

using more aggressive suction attachment. After the cut was made, the sample was covered in an OCT compound and flash frozen using liquid nitrogen. A cryotome was subsequently used to section the sample into 10 µm sections, which were photographed every five sections. No sections were collected for histology. Fig. 5-22 shows a cross-section photo taken during cryotome sectioning. The blue beads are visible on either side of, but not in the cut, suggesting that no significant quantities of beads are carried into the sample via the cutting jets.

These are preliminary tests. Further testing is needed to definitively evaluate whether bacteria are driven into the tissue. As a first step, 10 µm sections of the bead-seeded samples should be cut with the cryotome and inspected with a microscope in order to visualize and allow quantification of any beads that have been propagated into the sample. Similar testing should also be performed with fluorescent bacteria used instead of the polystyrene beads in order to verify that the microspheres are a valid approximation of bacterial behavior.

Chapter 6

Conclusions and Future Work

We have explored techniqued for debriding tissue with fluid jets and have shown that tissue sections can be excised by making two parallel cuts that intersect subsurface. A device employing two simultaneous cutting jets was designed and fabricated. When the two jets are aligned to impinge, most of their kinetic energy is dissipated into atomization. The fluid does not retain enough energy to cut after atomization, and the device is able to excise sample strips without perforating the deeper tissue. When making side-by-side cuts, the jets that intersect at a shallower angle leave a smoother resulting surface. Applying vacuum at the cutting location was effective both in holding the tissue for cutting and in evacuating debris. The pressure necessary to excise tissue depends both on the jet configuration and the sample properties. Cutting simulated sloughy tissue with 75 µm nozzles spaced 4 mm apart and the jets intersecting at 120° required 15 MPa of pressure, but cutting the same material with nozzles 2 mm apart and intersecting at 110° required only 10 MPa. To debride simulated hard eschar using this narrower configuration again required 15 MPa.

Use of the device in soft tissue caused water to inject into the sample. This water injection was reduced by translating the device more quickly during debridement, though sections were not reliably excised at faster speeds. Injection was also reduced by using small surgical blades to initiate incisions which the cutting jets then deep-

ened. Using this technique while applying vacuum, the required cutting pressure was 6 MPa in simulated slough using 75 µm nozzles spaced 2 mm apart and intersecting at 110°. The lowest injection levels were measured with this configuration employed without applying vacuum to have an average of $4.3\,L/m^2$ and a standard deviation of $4.7\,L/m^2$, higher than the desired $3\,L/m^2$. Substantial variation was observed between samples: 3 out of five samples tested with the pre-cutting blades and vacuum had injection levels in the same range observed for pre-cutting blades without vacuum, while due to tissue variations the two other samples had an elevated water injection level of $23.4\,Lm^2$ on average.

There are several options to further reduce water injection. One option is to position the blades to cut at a steeper angle. In the tested configuration, the blades were aligned with the nozzles and were close to tangential against the sample surface. The two blades entered from opposite directions, and downward force on the device was necessary to initiate incisions with both blades simultaneously. Because less water injection was measured when the blades cut more deeply, we expected that installing the blades more vertically will improve the both reduce water injection and improve behavior consistency between samples by increasing the reliability with which the blades make incisions.

A second option for reducing water injection is to add a component to the device that applies tension to the tissue being cut. Less force is required to cut tissue under tension, and so applying tension to the sample may reduced the required cutting pressure and therefore reduce the water injection.

Preliminary tests suggested that the debridement device was not driving bacteria into soft tissue. These tests, which used 1 µm dyed beads to simulate bacteria, should be repeated, and the samples should be sectioned and viewed through a microscope in order to count the individual beads propagated into the sample. As a final confirmation that the device does not propagate bacteria, the same test should again be repeated with the surface seeded with fluorescent bacteria instead of microbeads.

Further testing could also include debriding different tissue types, and correlating the cutting behavior to the material properties shown to be predictive in jet injection, such as Young's modulus.

Lastly, the device could be developed to incorporate a sensor to measure properties of the necrotic tissue and to modulate jet pressure accordingly. Actuating the device using linear Lorentz-force actuators instead of a pneumatic pump would give a direct means for controlling the jet pressure electrically based on sensor data.

Bibliography

[1] H. Brem, O. Stojadinovic, R. F. Diegelmann, H. Entero, B. Lee, I. Pastar, M. Golinko, H. Rosenberg, and M. Tomic-Canic, "Molemodel markers in patients with chronic wounds to guide surgical debridement," *Molecular Medicine*, vol. 13, no. 1-2, pp. 30–39, 2007.

[2] M. Augustin and K. Maier, "Psychosomatic aspects of chronic wounds," *Dermatology and Psychosomatics*, vol. 4, no. 1, 2003.

[3] S. Guo and L. DiPietro, "Factors affecting wound healing," *Journal of Dental Research*, vol. 89, no. 3, pp. 219–229, 2010.

[4] V. Falanga, H. Brem, and W. Ennis, "Maintenance debridement in the treatment of difficult-to-heal chronic wounds," *Ostomy/Wound Management*, vol. Supplement 2, no. 13, 2008.

[5] Z. Moore, "The important role of debridement in wound bed preparation," *Wounds International*, vol. 3, no. 2, 2012.

[6] A. G. Nusbaum, J. Gil, M. Rippy, B. Warne, J. Valdes, A. Claro, and S. C. Davis, "Effective method to remove wound bacteria: comparison of various debridement modalities in an *in vivo* porcine model," *Journal of Surgical Research*, vol. 176, no. 2, pp. 701–707, 2012.

[7] P. Martin, "Wound healing–aiming for perfect skin regeneration," *Science*, vol. 276, no. 75, pp. 75–80, 1997.

[8] G. S. Schultz, R. G. Sibbald, V. Falanga, E. A. Ayello, C. Dowsett, K. Harding, M. Romanelli, M. C. Stacey, L. Teot, and W. Vanscheidt, "Wound bed preparation: a systematic appraoch to wound management," *Wound Repair and Regeneration*, vol. 11, no. 2, pp. 1–28, 2003.

[9] A. Gosain and L. DiPietro, "Aging and wound healing," *World Journal of Surgery*, vol. 28, pp. 321–326, 2004.

[10] G. Schulz, R. Sibbald, and V. Falanga, "Wound bed preparation: A systematic approach to wound management," *Wound Repair and Regeneration*, vol. 11, no. S1, 2003.

[11] "Chronic wound assessment." Online, 2011.

[12] S. M. Hassinger, G. Harding, and M. D. Wongworawat, "High-pressure pulsatile lavage propagates bacteria into soft tissue," *Clinical Orthopaedics and Related Research*, vol. 439, pp. 27–31, 2005.

[13] G. Rodheaver, D. Pettry, J. Thacker, M. Edgerton, and R. Edlich, "Wound cleansing by high pressure irrigation," *Surgery, Gynecology and Obstetrics*, vol. 141, pp. 357–362, 1975.

[14] J. I. Boyd and M. D. Wongworawat, "High-pressure pulsatile lavage causes soft tissue damage," *Clinical Orthopaedics and Related Research*, no. 427, pp. 13–17, 2004.

[15] M. Granick, J. Boykin, R. Gamelli, G. Schultz, and M. Tenenhaus, "Toward a common language: surgical wound bed preparation and debridement," *Wound Repair and Regeneration*, vol. 19, pp. 506–19, 2006.

[16] T. J. B. Instituite., "debridement conservative sharp wound debridement for chronic wounds," *Wound Practice and Reseach*, vol. 19, pp. 29–31, 2011.

[17] R. Sibbald, D. Williamson, H. Orsted, K. Campbell, D. Keast, D. Drasner, and D. Sibbald, "Preparing the wound bed–debridement, bacterial balance and moisture balance," *Ostomy/Wound Management*, vol. 46, pp. 14–35, 2000.

[18] L. Ovington, "Hanging wet-to-dry dressings out to dry," *Home Health Nurse*, 2001.

[19] J. Dumvill, G. Worthy, and J. Bland, "Larval therapy for leg ulcers(venus ii): randomized controlled trial," *British Medical Journal*, vol. 338, p. 773, 2009.

[20] R. Gurunluoglu, "Experiences with waterjet hydrosurgery system in wound debridement," *World Journal of Emergency Surgery*, vol. 2, no. 10, 2007.

[21] E. A. Dion, E. MacKenzie, and R. Bevier, "Wound bed preparation," April 2010.

[22] T. Cubison, S. Pape, and S. Jeffry, "Dermal preservation using the versajet hydrosurgery system for debridement of paediatric burns," *Burns*, vol. 32, no. 714, 2006.

[23] "Versajet ii." Smith & Nephew, London. `http://www.smith-nephew.com`.

[24] G. Ostrovsky, "Versajet hydrosurgery system," *medGadget*, 2006. `http://www.medgadget.com/2006/09/versajet_hydros.html`.

[25] O. A. Shergold, N. A. Fleck, and T. S. King, "The penetration of a soft solid by a liquid jet, with application to the administration of a needle-free injection," *Journal of Biomechanics*, vol. 39, pp. 2593–2602, 2006.

[26] M. Mahvash and V. Hayward, "Haptic rendering of cutting: a fracture mechanics approach," *Journal of Haptics Research (www.haptics-e.org)*, vol. 2, p. 2001, 2001.

[27] J. Baxter and S. Mitragotri, "Jet-induced skin puncture and its impact on needle-free jet iinjection: Experimental studies and a predictive model," *Journal of Controlled Release*, vol. 106, pp. 361–373, 2005.

[28] F. Xu, *Introduction to Skin Biothermomechanics and Thermal Pain.* Science Press Beijing and Springer-Verlag Heidelberg, 2011.

[29] K. Chen and H. Zhou, "An experimental study and model validation of pressure in liquid needle-free injection," *International Journal of the Physical Sciences*, vol. 6, no. 7, pp. 1552–1562, 2011.

[30] J. Schramm-Baxter and S. Mitragotri, "Needle-free jet injection: dependence of jet penetration and dispersion in the skin on jet power," *Journal of Controlled Release*, 2004.

[31] Proceedings of the 28th IEEE, *The effect of jet parmeters of jet injection*, Sept 2006.

[32] A. Taberner, N. Hogan, and I. Hunter, "Needle-free jet injection using real-time controlled linear lorentz-force actuators," *Medical Engineering and Physics*, 2012.

[33] Maxpro Technologies, Fairview, PA. `http://www.maxprotech.com/`.

[34] "Zimmer pulsavac plus ac wound debridement system.." Zimmer Holdings, Warsaw, IN. `http://www.zimmer.com/`.

[35] Small Precision Tools Inc., Petaluma, CA. `http://www.smallprecisiontools.com/`.

[36] A. M. Cloutier, "Lorentz-force actuated needle-free injection for intratrympanic pharmaceutical delivery," Master's thesis, MIT, 2013.

[37] "Loctite brand." Henkel Corporation, Westlake, OH. `http://www.loctite.com/`.

[38] "Cpx1800 ultrasonic cleaner." Branson Ultrasonics Corporation, Danbury, CN. `http://www.emersonindustrial.com/en-US/branson/Pages/home.aspx/`.

[39] VWR International, Radnor, PA. `https://us.vwr.com/`.

[40] J. Black, M. Baharestani, S. Black, J. Cavazos, T. Conner-Kerr, L. Edsberg, B. Peirce, E. Rivera, and G. Schultz, "An overview of tissue types in pressure ulcers: A consensus panel recommendation," *Ostomy Wound Management*, vol. 56, no. 4, pp. 28–44, 2010.

[41] J. Ratanavaraporn, S. Kanokpanont, Y. Tabata, and S. Damrongsakkul, "Effects of acid type on physical and biological properties of collagen scaffolds," *Journal of Biomaterials Science, Polymer Edition*, vol. 19, no. 7, pp. 945–952, 2008.

[42] A. Kessler, H. Rosen, and S. Levenson, "Chromatographic fractionation of acetic acid-solubilized rat tail tendon collagen," *The Journal of Biological Chemistry*, vol. 235, no. 4, pp. 989–994, 1960.

[43] P. F. Davison, D. J. Cannon, and L. P. Andersson, "The effects of acetic acid on collagen corss-links," *Connective Tissue Research*, vol. 1, pp. 205–216, 1972.

[44] D. DiMaio and V. DiMaio, *Forensic Pathology.* CRC Press, second ed., 2001.

[45] "Occupational safety and health guideline for acetic acid."

[46] N. Ashgriz, *Handbook of Atomization and Sprays.* Springer, 2011.

[47] D. K. Giles, "Energy conversion and distribution in pressure atomization," *Transactions of the ASAE*, vol. 31, no. 6, pp. 1668–1673, 1679, 1988.

[48] S. Sinha and N. Cooling, "Simulation based education," *Australian Family Physician*, vol. 41, no. 12, pp. 985–988, 2012.

[49] S. Jones, P. G. Bowler, and M. Walker, "Antimicrobial activity of silver-containing dressings is influenced by dressing conformability with a wound surface," *Wounds*, vol. 17, no. 9, pp. 263–270, 2005.

[50] Autodesk, San Rafael, CA. `http://www.autodesk.com/`.

[51] MeshLab, Visual Computing Lab - ISTI - CNR. `http://meshlab.sourgeforce.net/`.

[52] "Matlab." MathWorks, Natick, MA. `http://www.mathworks.com/`.

[53] "Acetal resin delrin." DuPont, Wilmington, DE. `http://www.dupont.com/products-and-services/plastics-polymers-resins/thermoplastics/brands/delrin-acetal-resin.html`.

[54] Gast Manufacturing, Benton Harbor, MI. `http://www.gastmfg.com/`.

[55] J. T. Snarski and R. H. Birkhahn, "Non-operative management of a high-pressure water inection injury to the hand," *Canadian Journal of Emergency Medicine*, vol. 7, no. 2, pp. 124–126, 2005.

[56] Immunization Action Coalition, *Ask the experts: administering vaccines.* `http://www.immunize.org/askexperts/administering-vaccines.asp`.

[57] M. Gilchrist, S. Keenan, M. Curtis, M. Cassidy, G. Byrne, and M. Destrade, "Measuring knife stab penetration into skin simulant using a novel biaxial tension device," *Forensic Science International*, vol. 177, pp. 52–65, 2008.

[58] Polysciences, Inc., Warrington, PA. `http://www.polysciences.com/`.